Toward Aerodynamic Shape Optimization for the Design of Natural-Laminar-Flow Wings

Michael G.H. Piotrowski [1,2] David W. Zingg [2]

[1]Computational Aerosciences Branch
NASA Ames Research Center

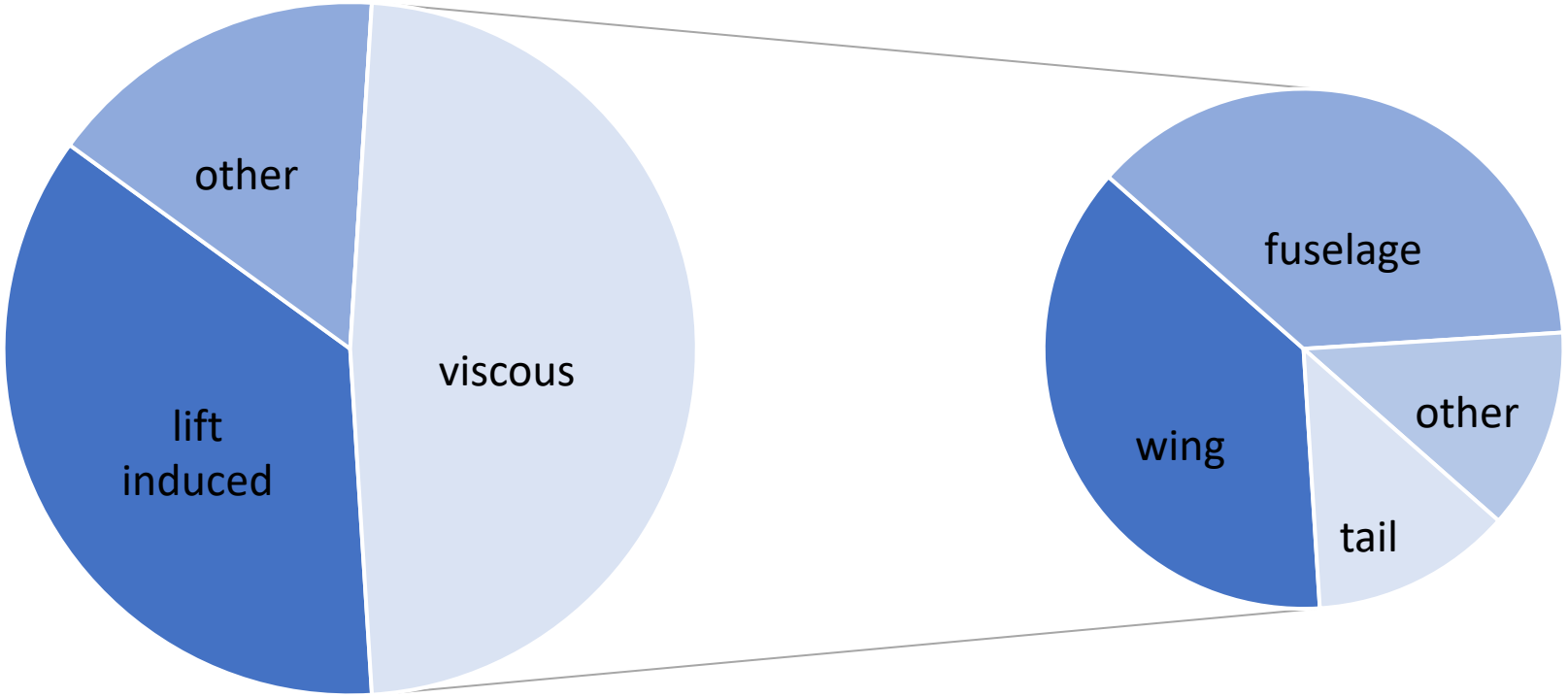
[2]University of Toronto Institute for Aerospace Studies

AMS Seminar

August 26th, 2021

Institute for Aerospace Studies
UNIVERSITY OF TORONTO
Centre for Research in Sustainable Aviation

Motivation

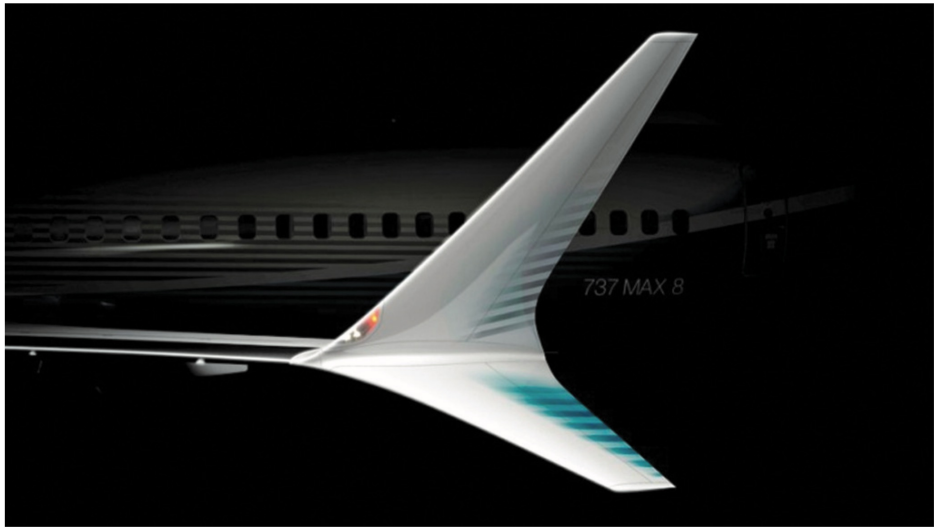


(a) Total Drag

(b) Viscous Drag

Drag Breakdown of a long-haul transport aircraft, Marec (2000). Natural-laminar-flow designs produce an increased laminar extent of the boundary layer resulting in a significant decrease in viscous drag.

Motivation



(a) Boeing 737-Max NLF Winglets[1]



(b) Boeing 787 NLF Nacelles[1]

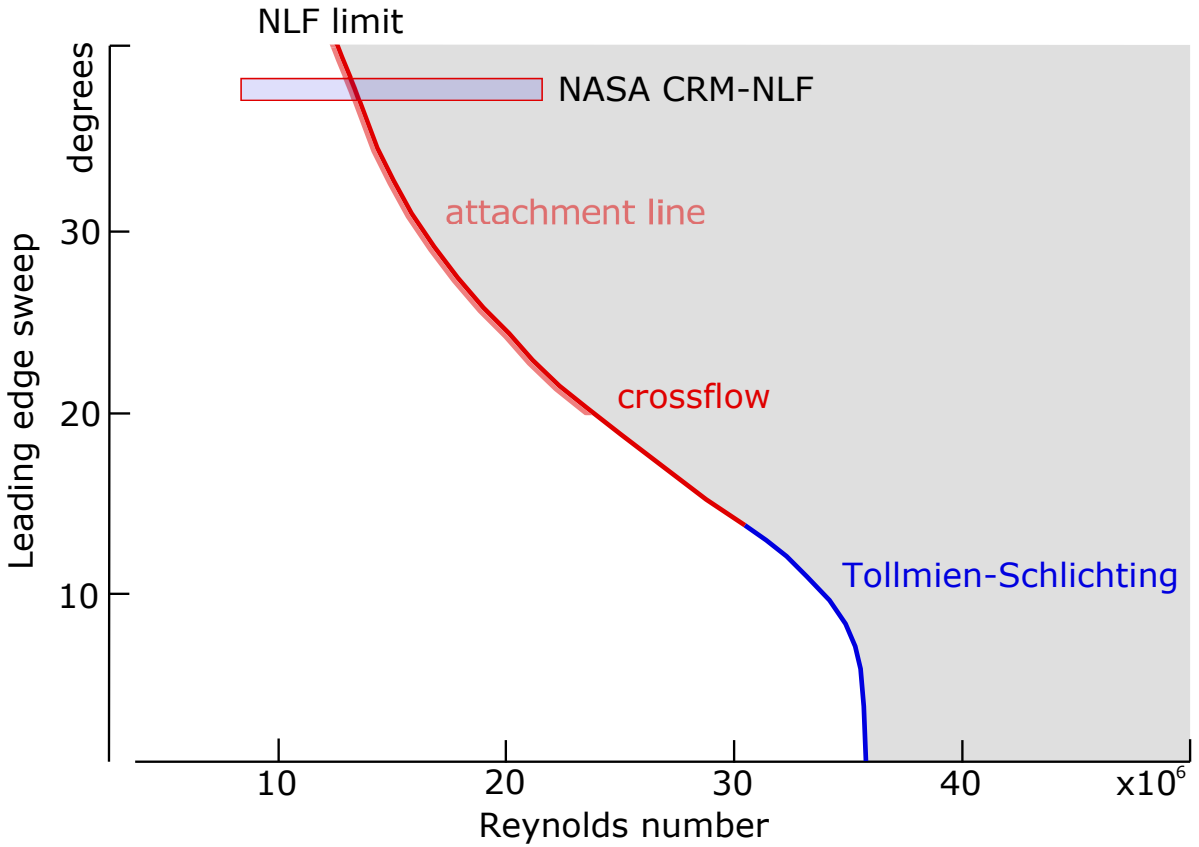
- The application of laminar flow control to commercial transport aircraft can reduce drag by approximately 10%[1].
- The application of NLF designs have so far been limited to low sweep and/or low Reynolds number configurations.



(c) HondaJet Fuselage and Wing[2]

[1] Malik et al. (2015)
[2] Fujino (2005)

Motivation



Historical barrier for NLF designs based on experiments with varying combinations of Reynolds number and wing leading-edge sweep angle, along with the primary transition mechanisms.

Objective

Objective: Produce strategies that enable the efficient prediction of boundary-layer transition in a high-fidelity RANS-based Newton-Krylov flow solver and discrete-adjoint gradient-based optimization algorithm to investigate the design of transonic NLF wings.

1. Extension of a three-dimensional RANS solver with a local laminar-turbulent transition prediction model.
2. Develop a framework for achieving deep, efficient convergence.
3. Validate model for transonic flow regimes typical of commercial transport aircraft.
4. Integrate in a discrete-adjoint gradient-based optimization algorithm and apply to drag-minimization studies.

Methodology: Aerodynamic Shape Optimization Algorithm

Jetstream: Efficient High-fidelity Aerodynamic Shape Optimization Algorithm

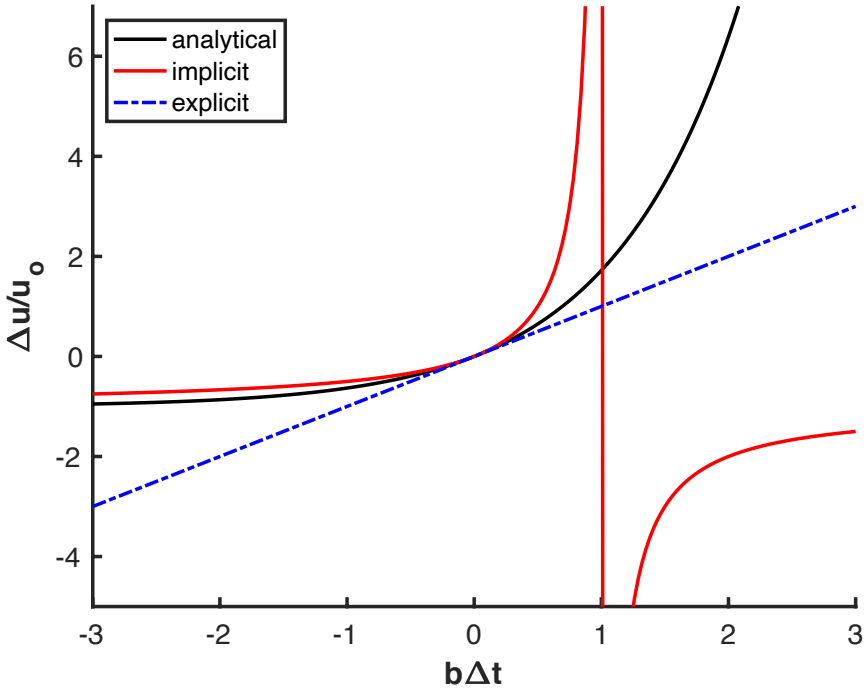
1. Geometry parameterization and control
   - Geometry parameterized and deformed using B-splines
   - Free-form deformation shape control
   - Linear-elasticity mesh movement

2. Parallel implicit Newton-Krylov-Schur RANS-based flow solver
   - SBP-SAT finite-difference spatial discretization with matrix-based dissipation
   - Pseudo-transient continuation time-marching strategy
   - FGMRES preconditioned with an approximate-Schur parallel preconditioner
   - RANS equations fully-coupled to the SA-sLM2015 Transition Model[1]
   - Source-term time stepping algorithm[1]

3. Discrete-adjoint gradient evaluation
   - Cost virtually independent of number of design variables
   - Flow adjoint system solved using GCROT
   - Design variables updated using SNOPT

[1]Piotrowski, M.G.H., and Zingg, D.W., "Smooth Local Correlation-Based Transition Model for the Spalart-Allmaras Turbulence Model" *AIAA Journal*, Vol. 59, No. 2 (2021), pp. 474-492, DOI: 10.2514/1.J059784

Methodology: Source-Term Time Stepping



Normalized solution update for the implicit and explicit treatment of a source term.

Lian et al. (2010) investigated implicit and explicit time marching strategies applied to a scalar convection equation with a source,

$$\frac{\partial u}{\partial t} + a\frac{\partial u}{\partial x} = bu$$

- Treating a source implicitly leads to an unbounded solution update.
- Implicit treatment of sinks produces a stable solution update.
- Explicit treatment of sources results in linear solution growth.

- The local time step is restricted to ensure the following source-term time step (STTS) condition is met,

$$\lambda_{\text{source}}\Delta t^{(n)}_{j,k,m} \leq 0.5, \qquad \mathcal{A}_{\text{source}} = \begin{bmatrix} \frac{\partial \mathcal{S}_{\tilde{\nu}}}{\partial \tilde{\nu}} & \frac{\partial \mathcal{S}_{\tilde{\nu}}}{\partial \gamma} & \frac{\partial \mathcal{S}_{\tilde{\nu}}}{\partial \tilde{Re}_{\theta t}} \\ \frac{\partial \mathcal{S}_{\gamma}}{\partial \tilde{\nu}} & \frac{\partial \mathcal{S}_{\gamma}}{\partial \gamma} & \frac{\partial \mathcal{S}_{\gamma}}{\partial \tilde{Re}_{\theta t}} \\ \frac{\partial \mathcal{S}_{\tilde{Re}_{\theta t}}}{\partial \tilde{\nu}} & \frac{\partial \mathcal{S}_{\tilde{Re}_{\theta t}}}{\partial \gamma} & \frac{\partial \mathcal{S}_{\tilde{Re}_{\theta t}}}{\partial \tilde{Re}_{\theta t}} \end{bmatrix}.$$

Methodology: Local Correlation-based Transition Models

SA-LM2015 Transition Model[1]

- LM2009 (Langtry and Menter 2009) and LM2015 (Langtry et al 2015) empirical correlations coupled with the SA turbulence model
- Novel coupling maintains a fully-local formulation
- Accurately predicts natural, bypass, separation-induced transition and transition due to stationary crossflow instabilities

SA-sLM2015 Transition Model[1]

- Approximations to discontinuous and stiff source-term functions introduced
- Smooth-variant improves numerical behaviour and provides a smooth design space

SA-sLM2015cc Transition Model[2]

- LM2009 and LM2015 empirical correlations developed based on results from low Mach number experiments and stability analysis
- Compressibility corrections derived based on results from stability analysis and the compressible AHD criterion
- Includes the stabilizing effects of compressibility in the natural and crossflow-induced transition correlations

[1]Piotrowski, M.G.H., and Zingg, D.W., "Smooth Local Correlation-Based Transition Model for the Spalart-Allmaras Turbulence Model" *AIAA Journal*, Vol. 59, No. 2 (2021), pp. 474-492, DOI: 10.2514/1.J059784

[2]Piotrowski, M.G.H., and Zingg, D.W., "Compressibility Corrections to Extend a Smooth Local Correlation-Based Transition Model to Transonic Flows" *Submitted*

Methodology: SA-LM2015 Transition Model

The SA-LM2015 transition model consists of three transport equations. Discontinuous and problematic functions in the LM2015 source terms are highlighted in red. Approximations to these terms are introduced in the smooth-variant of the model, SA-sLM2015.

- Intermittency;

$$\frac{\partial \gamma}{\partial t} + u_j \frac{\partial \gamma}{\partial x_j} = P_\gamma - E_\gamma + \frac{1}{Re}\frac{\partial}{\partial x_j}\left[\left(\nu + \frac{\nu_t}{\sigma_f}\right)\frac{\partial \gamma}{\partial x_j}\right],$$
$$P_\gamma = c_{a1} F_{\text{length}} F_{\text{onset}} \Omega \sqrt{\gamma}(1 - c_{e1}\gamma),$$
$$E_\gamma = c_{a2} F_{\text{turb}} \Omega \gamma (c_{e2}\gamma - 1),$$

- Transition-onset momentum thickness Reynolds number;

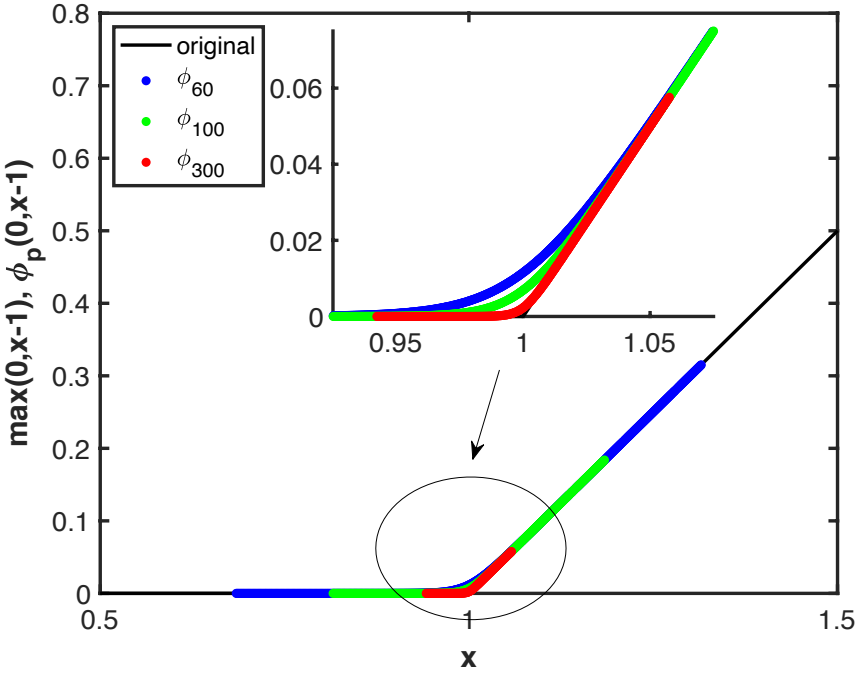
$$\frac{\partial \tilde{Re}_{\theta t}}{\partial t} + u_j \frac{\partial \tilde{Re}_{\theta t}}{\partial x_j} = P_{\theta t} + D_{\text{scf}} + \frac{1}{Re}\frac{\partial}{\partial x_j}\left[\sigma_{\theta t}(\nu + \nu_t)\frac{\partial \tilde{Re}_{\theta t}}{\partial x_j}\right],$$
$$P_{\theta t} = \frac{c_{\theta t}}{\mathrm{t}}(Re_{\theta t} - \tilde{Re}_{\theta t})(1 - F_{\theta t}),$$
$$D_{\text{scf}} = \frac{c_{\theta t}}{\mathrm{t}} c_{\text{crossflow}} \min(Re_{\text{scf}} - \tilde{Re}_{\theta t}, 0)(F_{\theta t}),$$

- Modified eddy viscosity;

$$\frac{\partial \tilde{\nu}}{\partial t} + u_j \frac{\partial \tilde{\nu}}{\partial x_j} = P_{\tilde{\nu}} - D_{\tilde{\nu}} + \frac{1}{\sigma Re}\left[\frac{\partial}{\partial x_j}\left((\nu + \tilde{\nu})\frac{\partial \tilde{\nu}}{\partial x_j}\right) + c_{b2}\frac{\partial \tilde{\nu}}{\partial x_i}\frac{\partial \tilde{\nu}}{\partial x_i}\right],$$
$$P_{\tilde{\nu}} = \gamma \frac{c_{b1}}{Re}\tilde{S}\tilde{\nu}; \quad D_{\tilde{\nu}} = \frac{c_{w1} f_w}{Re}\left(\frac{\tilde{\nu}}{d}\right)^2.$$

Smooth Approximations: Min/Max Operators

The LM2015 transition model source terms contain min/max operators that produce discontinuous gradients. These are approximated using a modified form of an exponential penalty function[1].



max(0,x-1) approximated using exponential penalty functions with various values for p.

$$\phi_p(x) \triangleq g_1(x) + \frac{\log\left(1 + \exp(p(g_2(x) - g_1(x)))\right)}{p}$$

$$\phi_{\text{switch}} \triangleq -\frac{\log(|p| \cdot p_{\text{switch}})}{|p|}$$

- Similar to a KS function for constraint aggregation.
- The proximity switch prevents numerical overflow and underflow.

Institute for Aerospace Studies
UNIVERSITY OF TORONTO
Centre for Research in Sustainable Aviation

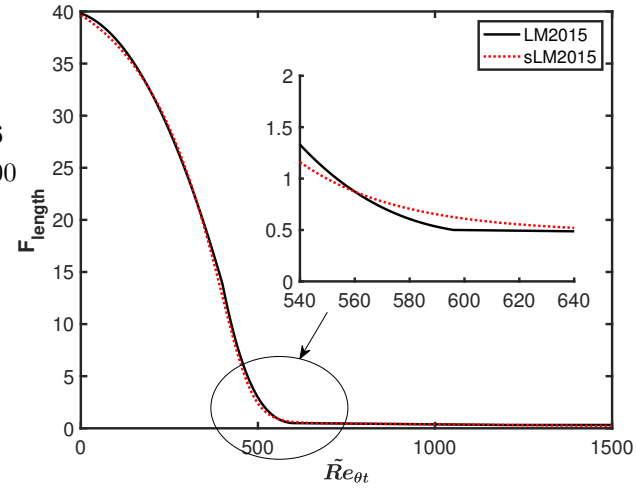
[1]Piotrowski, M.G.H., and Zingg, D.W., "Smooth Local Correlation-Based Transition Model for the Spalart-Allmaras Turbulence Model" *AIAA Journal*, Vol. 59, No. 2 (2021), pp. 474-492, DOI: 10.2514/1.J059784

Smooth Approximations: Case Dependent Functions

LM2015 transition model contains case dependent functions, which similarly are non-differentiable. Smooth approximations are introduced in the sLM2015 transition model.

Original:

$$F_{\text{length}} = \begin{cases} 398.189 \cdot 10^{-1} + (-119.270 \cdot 10^{-4})\tilde{Re}_{\theta t} + (-132.567 \cdot 10^{-6})\tilde{Re}_{\theta t}^2 & \tilde{Re}_{\theta t} < 400 \\ 263.404 + (-1.24)\tilde{Re}_{\theta t} + (194.548 \cdot 10^{-5})\tilde{Re}_{\theta t}^2 + (-101.695 \cdot 10^{-8})\tilde{Re}_{\theta t}^3 & 400 \leq \tilde{Re}_{\theta t} < 596 \\ 0.5 - (\tilde{Re}_{\theta t} - 596.0) \cdot 3 \cdot 10^{-4}) & 596 \leq \tilde{Re}_{\theta t} < 1200 \\ 0.3188 & 1200 \leq \tilde{Re}_{\theta t} \end{cases}$$



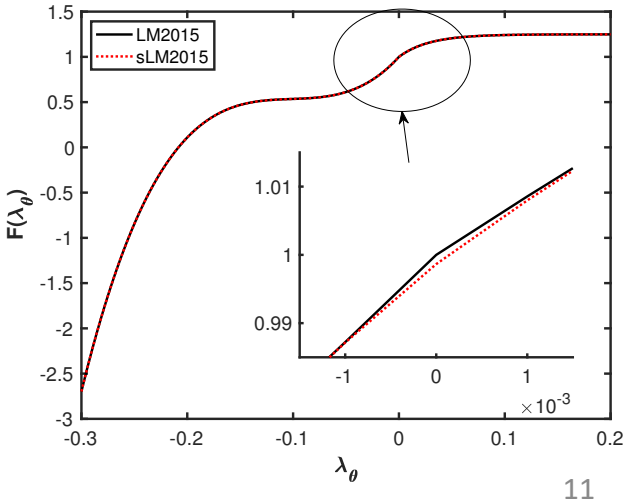
Smooth:

$$F_{\text{length1}} = \exp(-3 \cdot 10^{-2}(\tilde{Re}_{\theta t} - 460)),$$

$$F_{\text{length}} = 44 - \frac{44 - (0.50 - 3 \cdot 10^{-4}(\tilde{Re}_{\theta t} - 596))}{(1 + F_{\text{length1}})^{\frac{1}{6}}}$$

Original:

$$F(\lambda_\theta) = \begin{cases} 1 - [-12.986\lambda_\theta - 123.66\lambda_\theta^2 - 405.689\lambda_\theta^3]e^{-[\frac{Tu}{1.5}]^{1.5}} & \lambda_\theta \leq 0, \\ 1 + 0.275[1 - e^{[-35\lambda_\theta]}]e^{-[\frac{Tu}{0.5}]} & \lambda_\theta > 0, \end{cases}$$



Smooth:

$$F(\lambda_\theta)_1 = 1 + 0.275[1 - e^{[-35\lambda_\theta]}]e^{-[\frac{Tu}{0.5}]}$$

$$F(\lambda_\theta)_2 = \phi_{300}(F(\lambda_\theta)_1, 1)$$

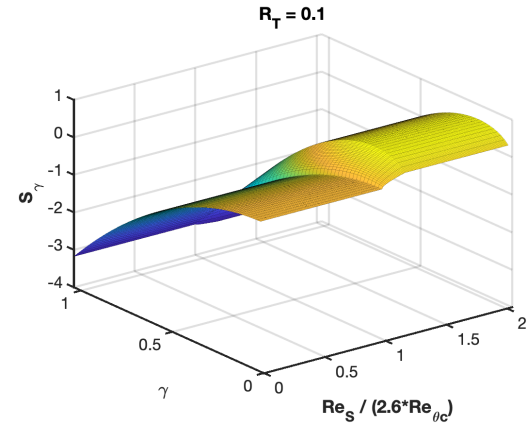
$$F(\lambda_\theta)_3 = 1 - [-12.986\lambda_\theta - 123.66\lambda_\theta^2 - 405.689\lambda_\theta^3]e^{-[\frac{Tu}{1.5}]^{1.5}}$$

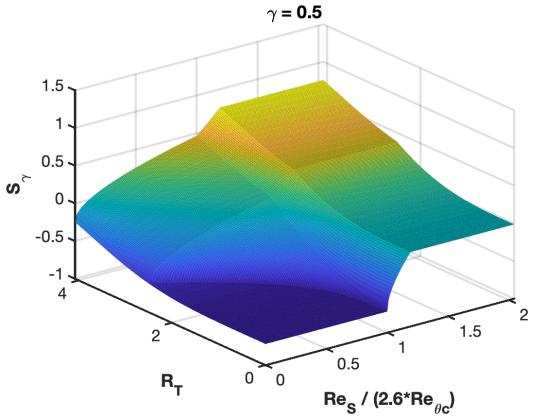
$$F(\lambda_\theta) = \phi_{-300}(F(\lambda_\theta)_2, F(\lambda_\theta)_3)$$

Smooth Approximations: Intermittency Source Terms

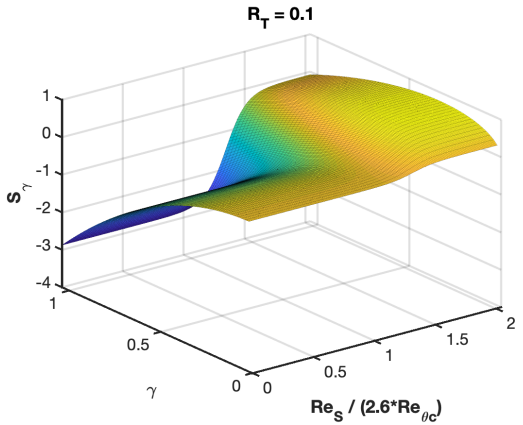
The intermittency source terms contain discontinuous and stiff functions. Smooth approximations are introduced, and the source terms are reformulated to reduce numerical stiffness[1].

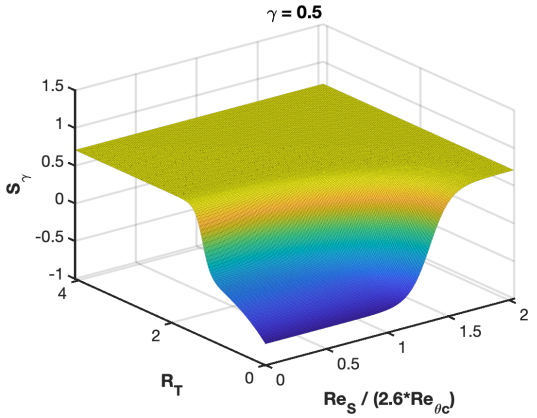
SA-LM2015





SA-sLM2015





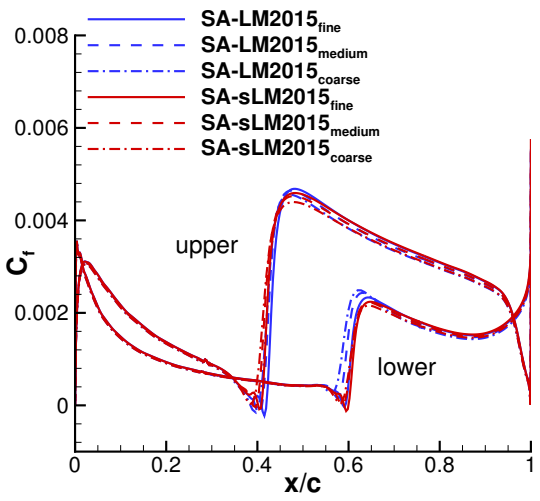
- The new source term formulation cannot predict boundary-layer re-laminarization.
- For the flows of interest re-laminarization is unlikely to be encountered.

Institute for Aerospace Studies
UNIVERSITY OF TORONTO
Centre for Research in Sustainable Aviation

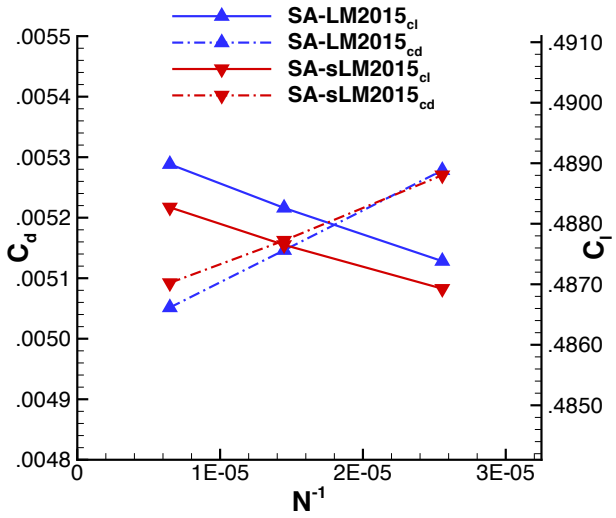
[1]Piotrowski, M.G.H., and Zingg, D.W., "Smooth Local Correlation-Based Transition Model for the Spalart-Allmaras Turbulence Model" *AIAA Journal*, Vol. 59, No. 2 (2021), pp. 474-492, DOI: 10.2514/1.J059784

Subsonic Validation: NLF-0416 Airfoil

M = 0.10 Tu = 0.15%
α = -6 - 6°
Re = 4.00x10^6

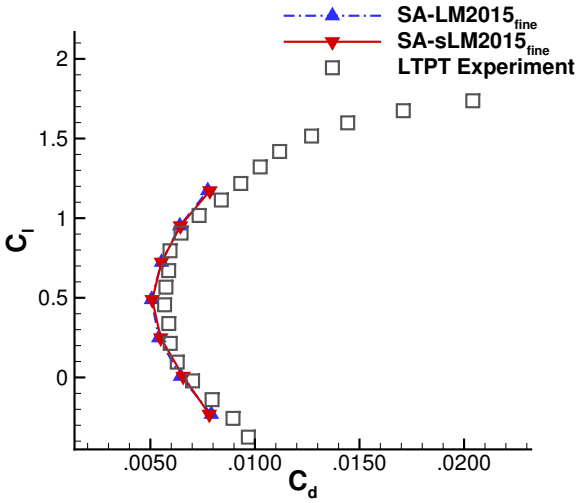


(a) Skin friction profiles

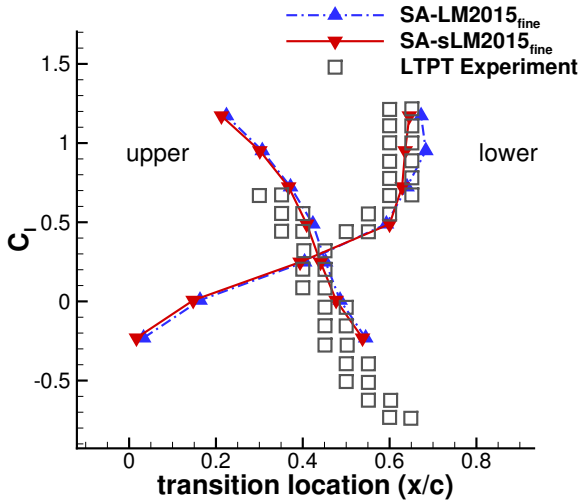


(b) Force convergence

- Grid convergence histories at 0° angle of attack.
- Smooth-variant, SA-sLM2015, produces a shallower grid convergence curve for drag.



(c) Drag polar

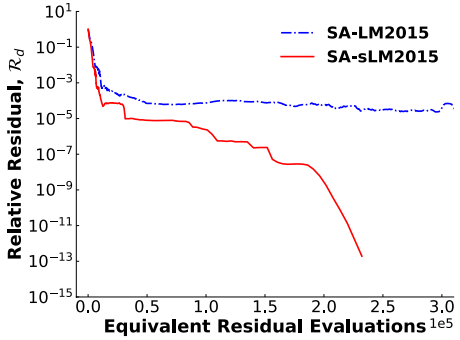


(b) Transition locations

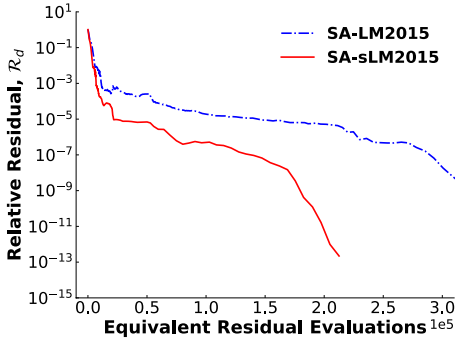
- Alpha sweep on fine grid.
- Smooth-variant agrees well with the original model and with experiment.

Subsonic Validation: NLF-0416 Airfoil

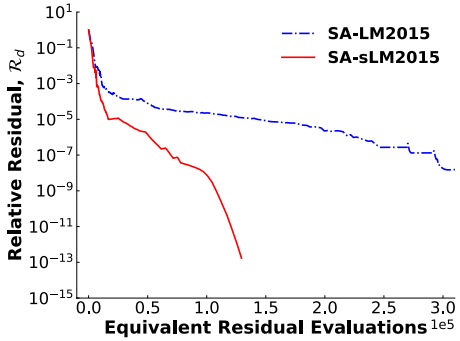
M = 0.10 Tu = 0.15%
α = -6 - 6°
Re = 4.00x10^6



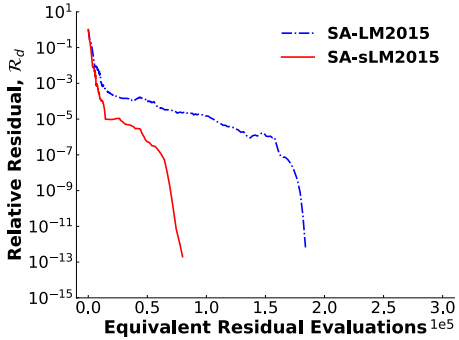
(a) -6°



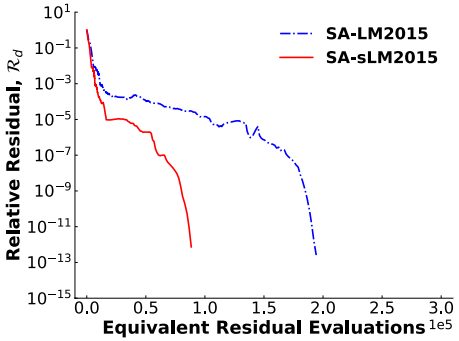
(b) -4°



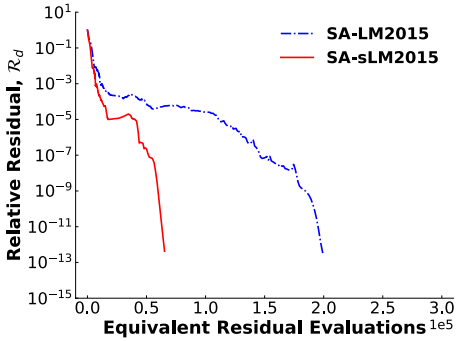
(c) -2°



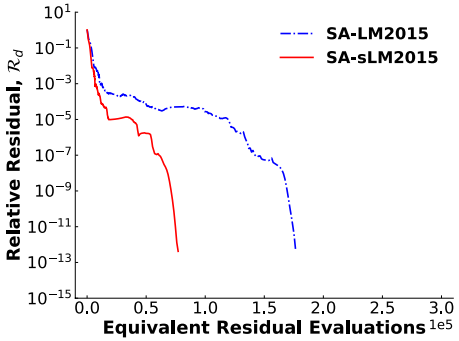
(d) 0°



(e) 2°



(f) 4°

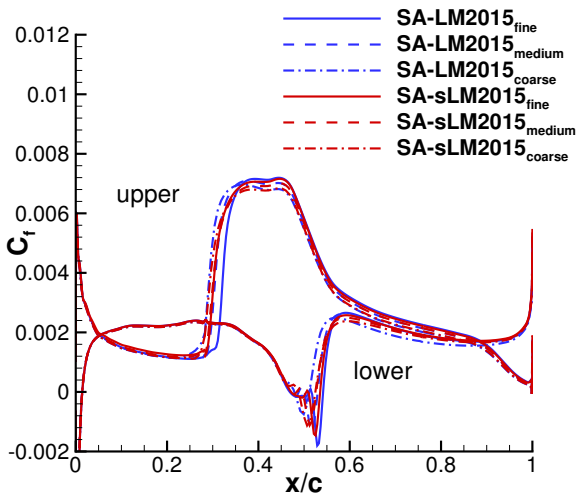


(g) 6°

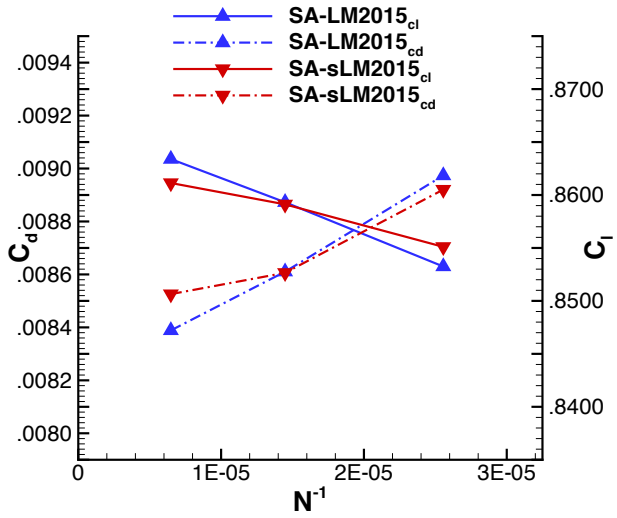
- The smooth-variant, SA-sLM2015, significantly reduces the computational cost required to achieve machine-zero convergence relative to the original model.

Subsonic Validation: S809 Airfoil

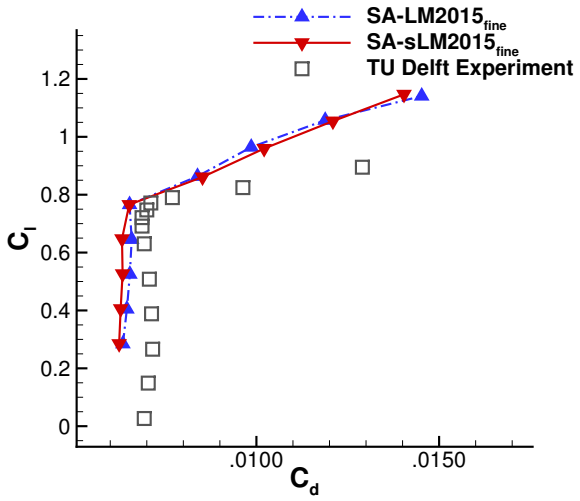
M = 0.10 Tu = 0.07%
α = 1 - 9°
Re = 2.00x10^6



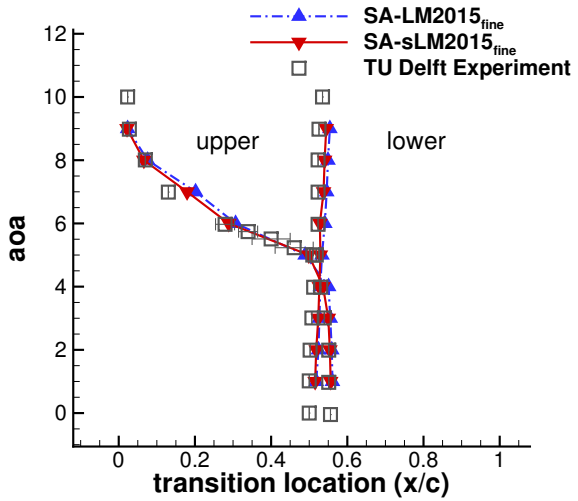
(a) Skin friction profiles



(b) Force convergence



(c) Drag polar



(b) Transition locations

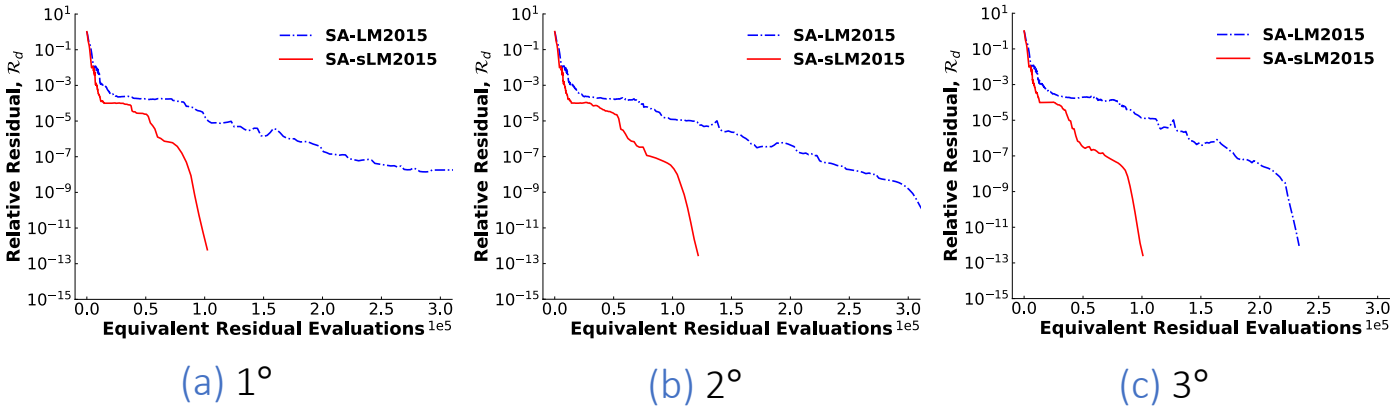
- Grid convergence histories at 6° angle of attack.
- Smooth-variant, SA-sLM2015, produces a shallower grid convergence curve for both lift and drag.

- Alpha sweep on fine grid.
- Smooth-variant agrees well with the original model and with experiment.

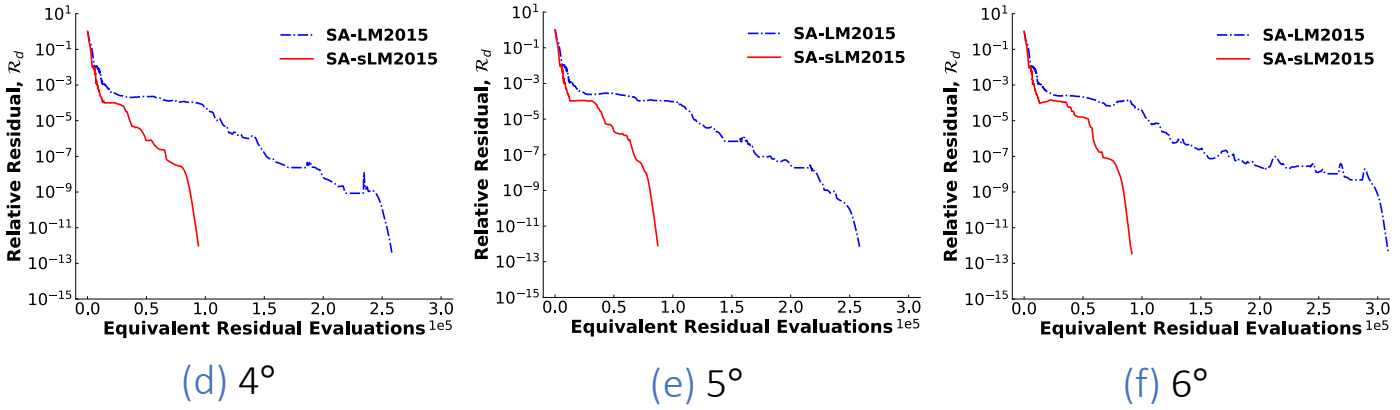
Subsonic Validation: S809 Airfoil

M = 0.10 Tu = 0.07%
α = 1 - 9°
Re = 2.00x10^6

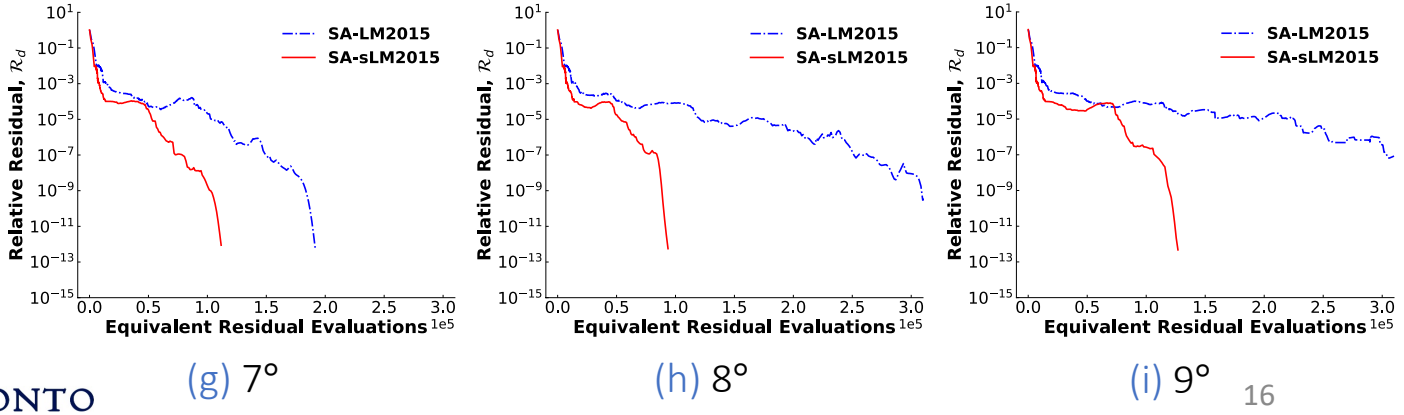
- SA-sLM2015 model converges with reduced computational cost.



(a) 1° (b) 2° (c) 3°



(d) 4° (e) 5° (f) 6°



(g) 7° (h) 8° (i) 9°

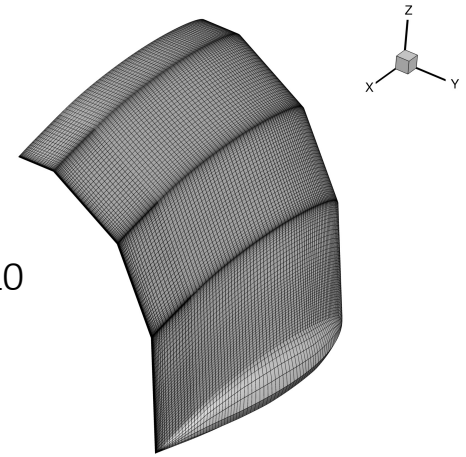
Institute for Aerospace Studies
UNIVERSITY OF TORONTO
Centre for Research in Sustainable Aviation

Subsonic Validation: Sickle Wing

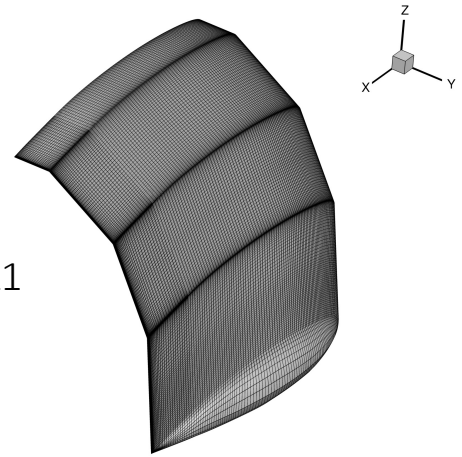
M = 0.16 Tu = 0.17%
α = -2.6° h_{rms} = 9.78x10^{-6}m
Re = 2.75x10^{6}

SA-LM2015 and SA-sLM2015 transition models validated using the TU Braunschweig Sickle Wing subsonic transition test case (Petzold and Radespiel 2015).

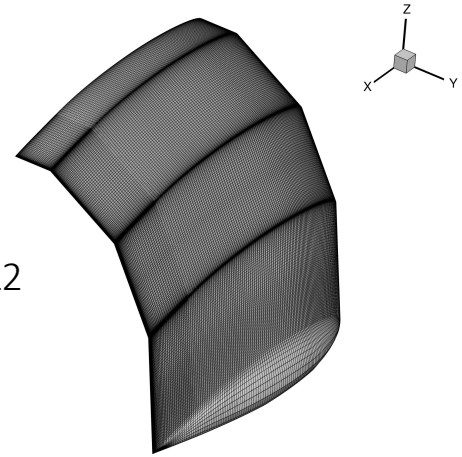
L0



L1



L2



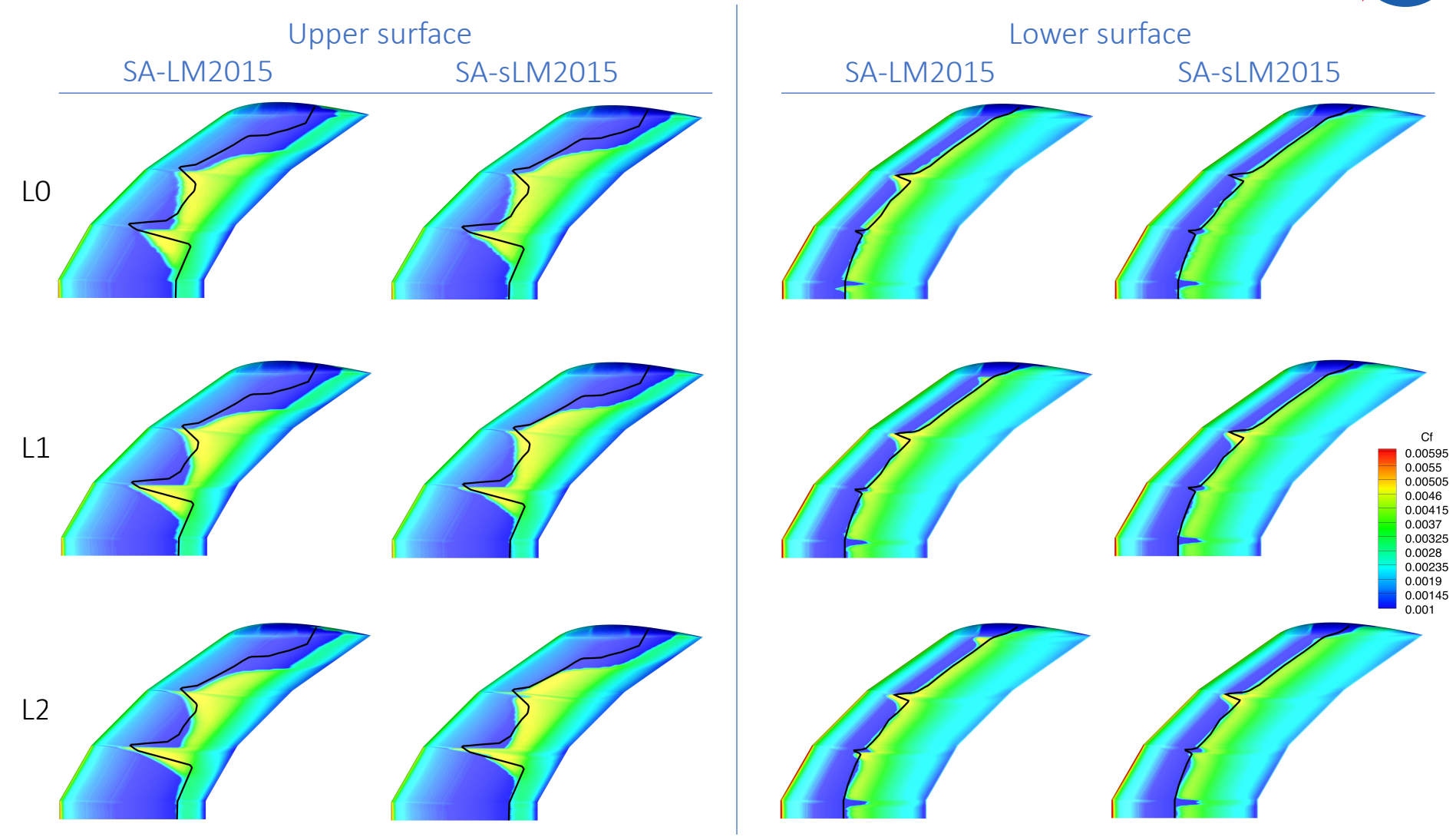
grid level	total node count, N	N-span	N-chord	Δs (chord)	average/maximum $y+$
L0	2.32×10^6	171	111	7.81×10^{-6}	0.70/2.64
L1	5.19×10^6	217	139	6.02×10^{-6}	0.54/1.55
L2	10.19×10^6	273	175	4.29×10^{-6}	0.39/1.13

- Full details of the range of two- and three-dimensional subsonic transition test cases can be found in Piotrowski and Zingg (2021)[1].

[1]Piotrowski, M.G.H., and Zingg, D.W., "Smooth Local Correlation-Based Transition Model for the Spalart-Allmaras Turbulence Model" *AIAA Journal*, Vol. 59, No. 2 (2021), pp. 474-492, DOI: 10.2514/1.J059784

Subsonic Validation: Sickle Wing

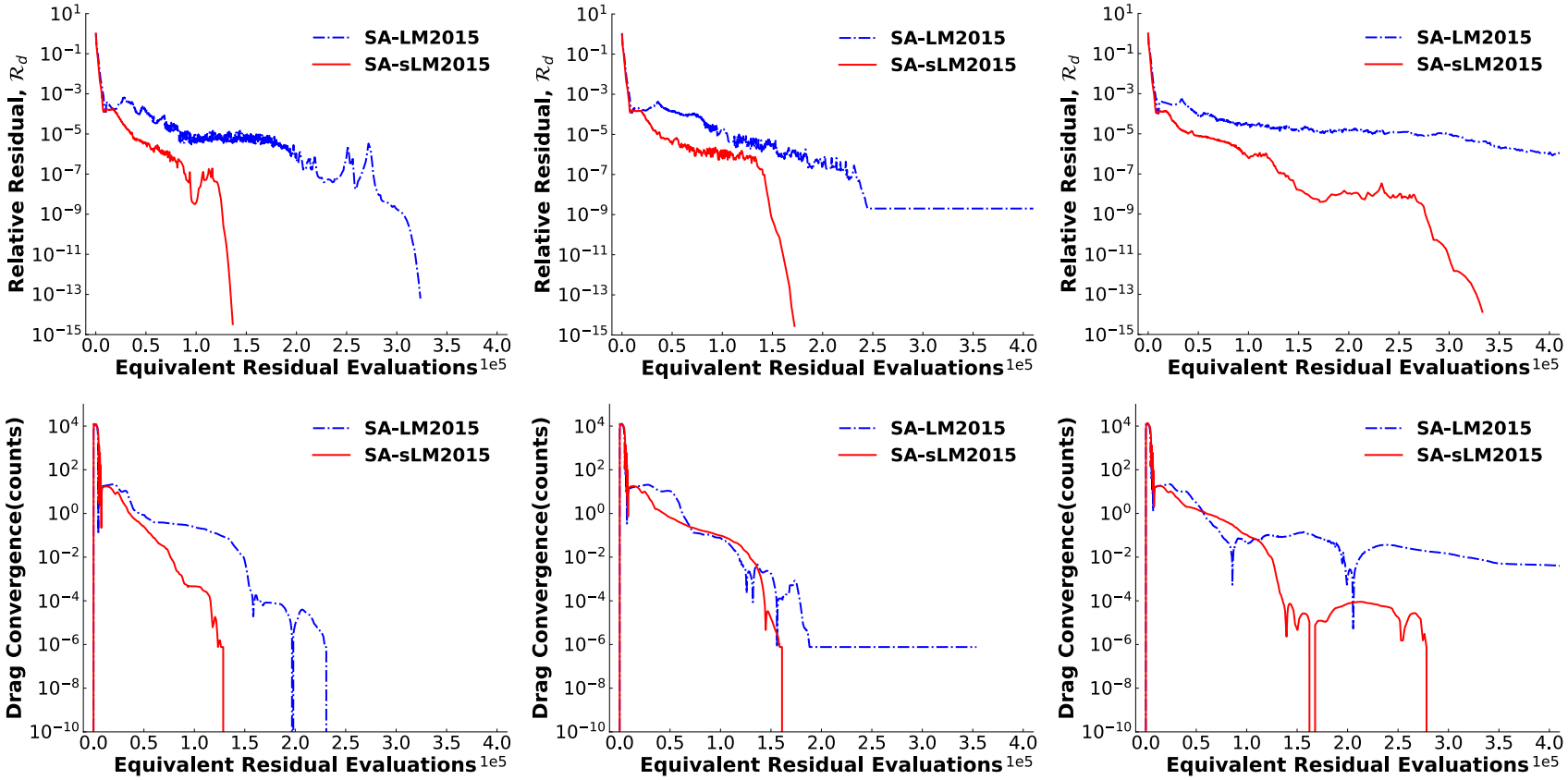
M = 0.16 Tu = 0.17%
α = -2.6° h_{rms} = 9.78x10^{-6}m
Re = 2.75x10^{6}



- Skin-friction profiles produced by the SA-LM2015 and SA-sLM2015 transition models overlaid with the experimental results, Petzold and Radespiel (2015).
- Both transition models produce transition fronts that agree well with experiment.

Subsonic Validation: Sickle Wing

M = 0.16 Tu = 0.17%
α = -2.6° h_{rms} = 9.78x10^{-6}m
Re = 2.75x10^{6}

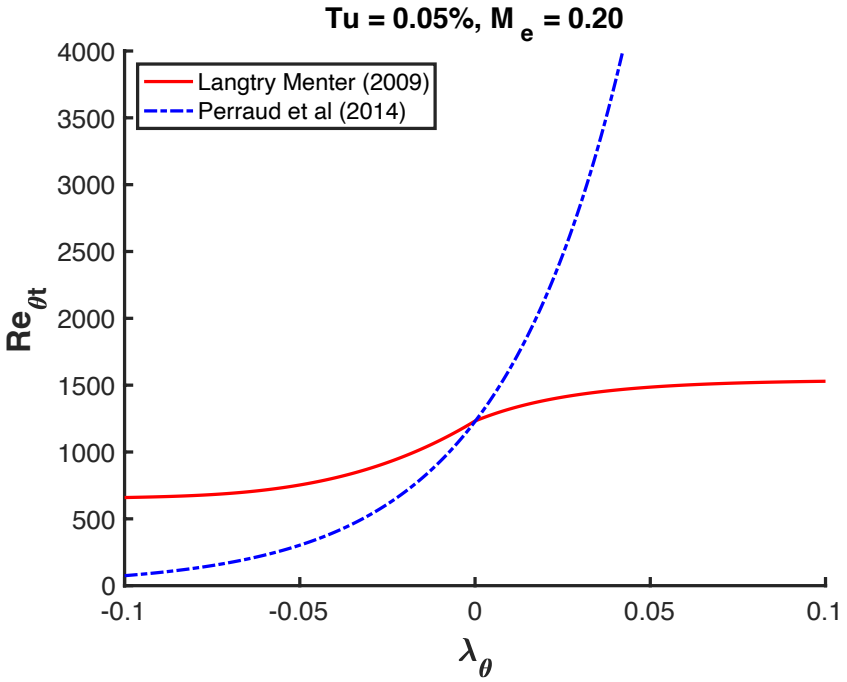


(a) L0 (b) L1 (c) L2

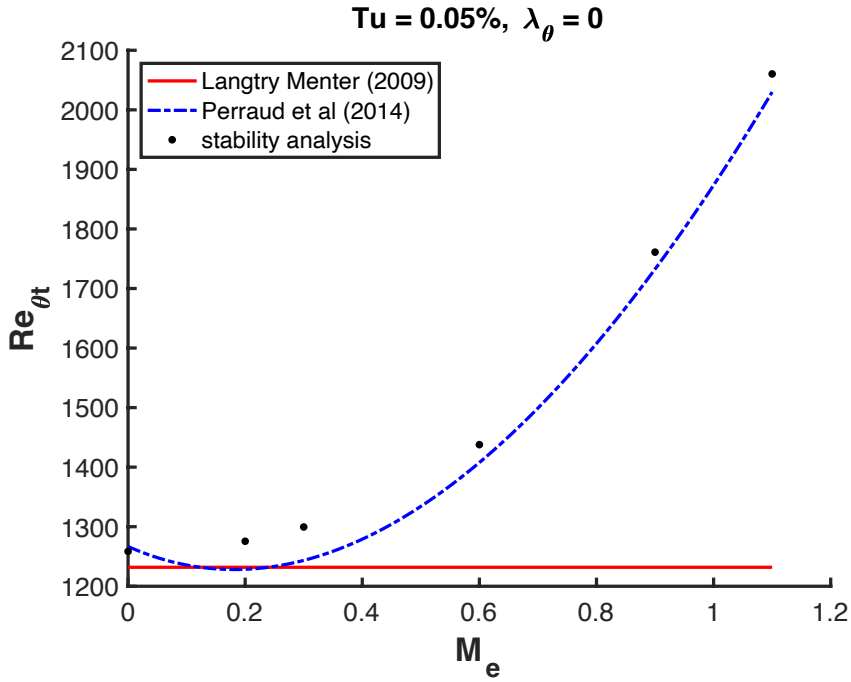
- The smooth SA-sLM2015 transition model consistently produces improved numerical behaviour.
- Reduced computational cost and improved robustness.

Compressibility Corrections: TS Instabilities

Perraud et al (2014) developed a simplified model based on the database of linear stability theory results that was used to create the compressible extension to the AHD criterion.



(a) Effects of pressure gradient

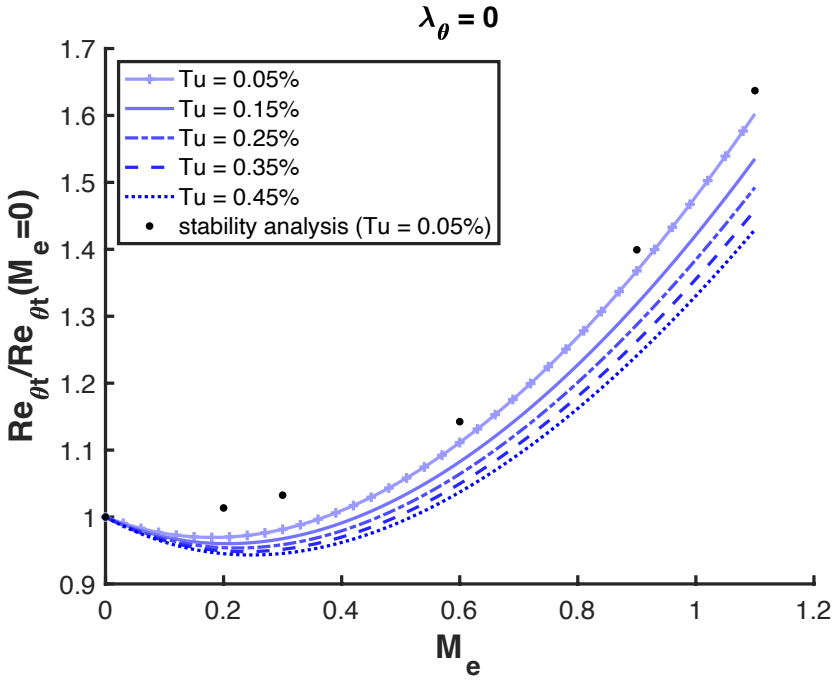


(b) Effects of flow compressibility

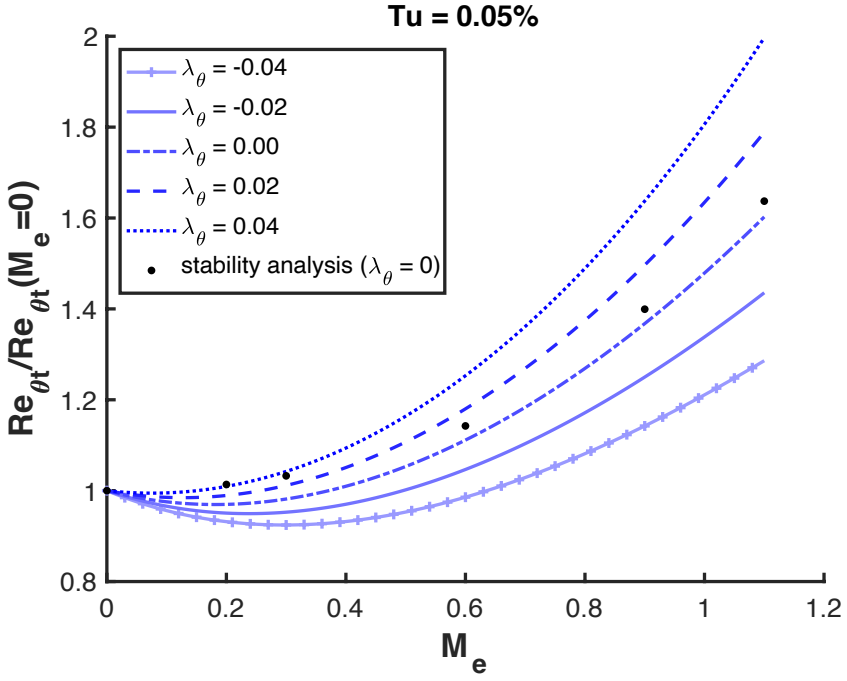
- Difference in sensitivity to pressure gradient may be due to the different pressure gradient parameter formulations.
- Langtry-Menter correlations do not include the stabilizing effect of flow compressibility on Tollmien-Schlichting (TS) instabilities.

Compressibility Corrections: TS Instabilities

The stability-based model of Perraud et al. (2014) can be used to better understand the relationship between flow compressibility, turbulence intensity, and pressure gradient.



(a) Turbulence intensity

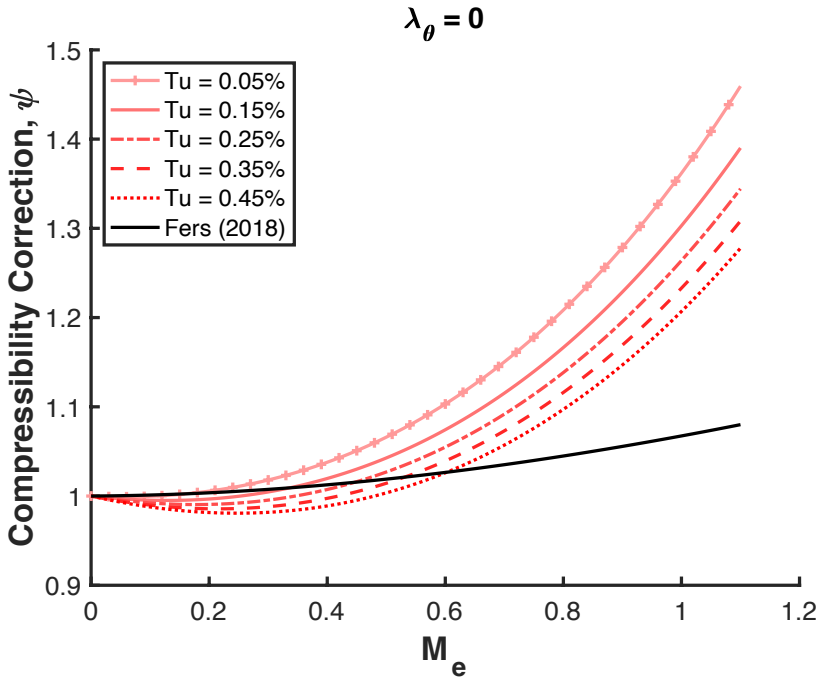


(b) Pressure gradient

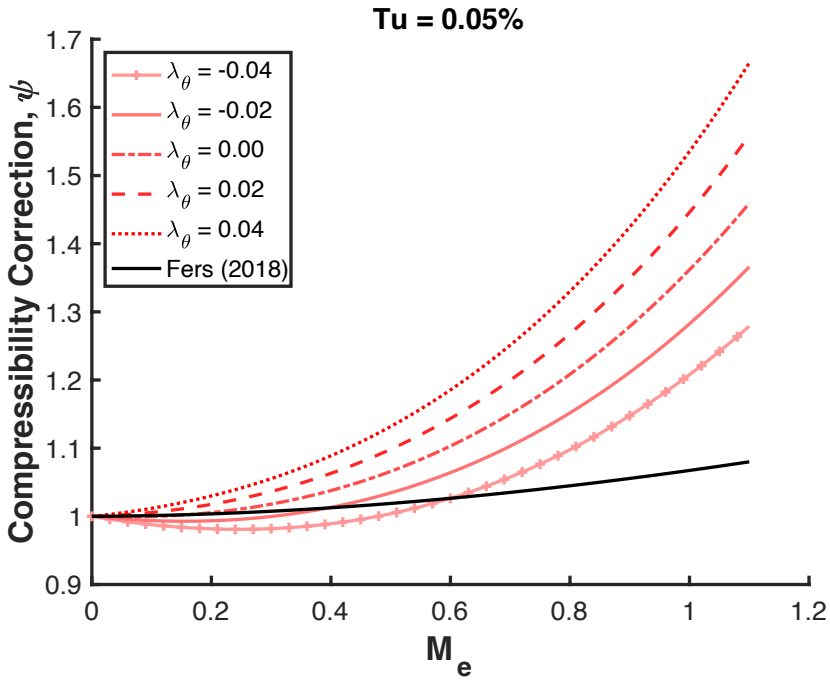
- Flow compressibility is most relevant at the high Reynolds number and low turbulence intensity conditions typical of commercial transport aircraft.

Compressibility Corrections: TS Instabilities

A compressibility correction[2] for Tollmien-Schlichting instabilities was developed and is applied to the Langtry-Menter (2009) empirical correlations.



(a) Turbulence intensity



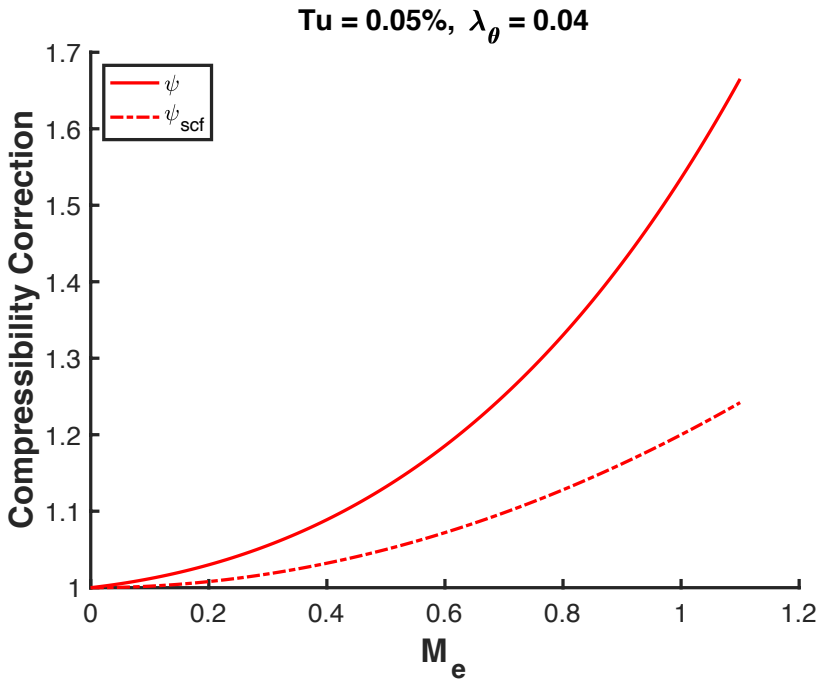
(b) Pressure gradient

- The correction by Fers (2018) was developed to account for the effects of flow compressibility on boundary-layer velocity profiles.

[2]Piotrowski, M.G.H., and Zingg, D.W., "Compressibility Corrections to Extend a Smooth Local Correlation-Based Transition Model to Transonic Flows" *Submitted*

Compressibility Corrections: SCF Instabilities

The local helicity-based stationary crossflow (SCF) instability correlation developed by Langtry et al (2015) is based on low Mach number results from experiment and stability analysis.



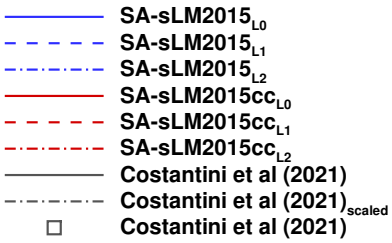
- Crossflow instabilities, which are dominated by the properties of the inflection point, are much less influenced by compressibility (Dagenhart 1981).
- Stabilizing effects of compressibility can be included using Malik's compressibility correction (Malik 1999);

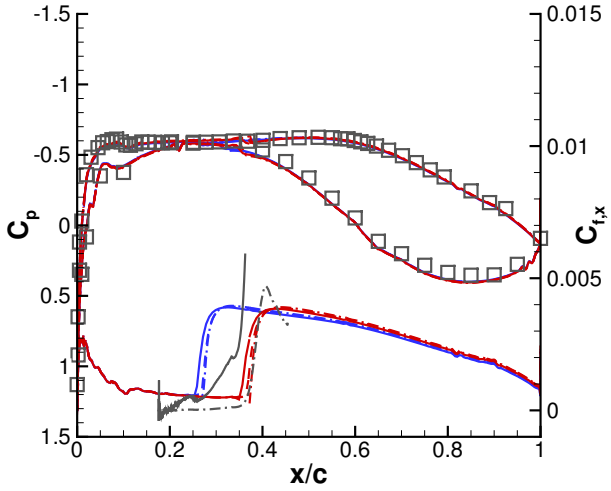
$$Re_{\text{scf}} = Re_{\text{scf}}\left(1 + \frac{\gamma - 1}{2} M_e^2\right).$$

Transonic Validation: VA-2 Airfoil

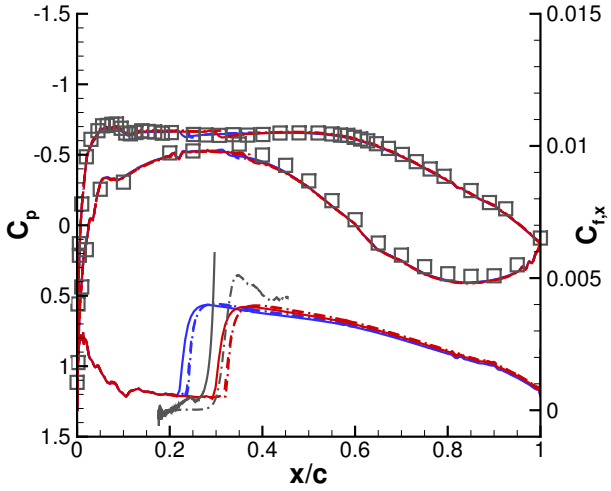
Alpha Sweep: Cross-Sectional Profiles

M = 0.71 Tu = 0.25%
α = -0.4 - 2.0°
Re = 10.0×10^6



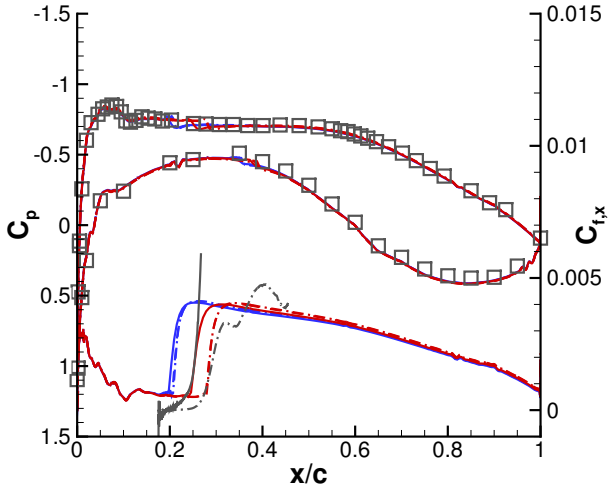


(a) -0.4 degrees

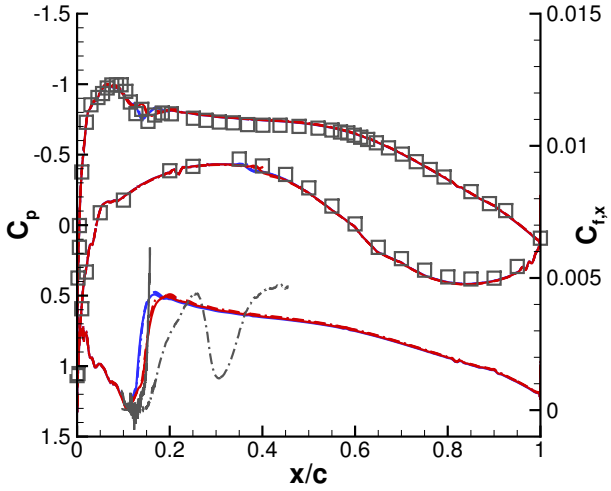


(b) 0 degrees

- Upper surface skin friction determined using a luminescent oil-film method (Costantini 2021).
- The relationship between the stabilizing effect of flow compressibility and pressure gradient is evident.



(c) 0.4 degrees



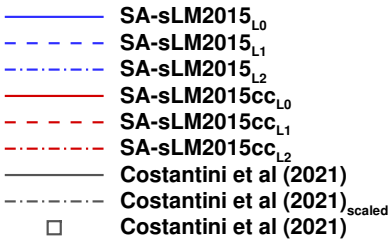
(d) 0.8 degrees

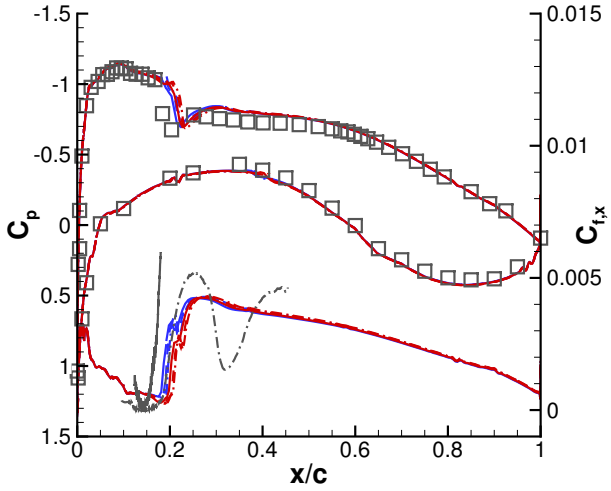
Institute for Aerospace Studies
UNIVERSITY OF TORONTO
Centre for Research in Sustainable Aviation

Transonic Validation: VA-2 Airfoil

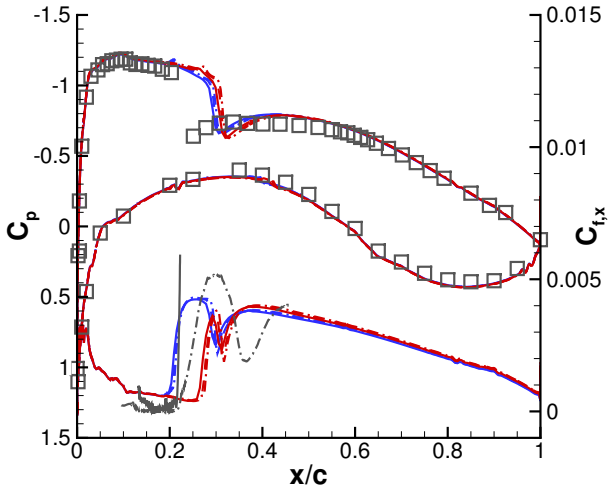
Alpha Sweep: Cross-Sectional Profiles

M = 0.71 Tu = 0.25%
α = -0.4 - 2.0°
Re = 10.0×10^6



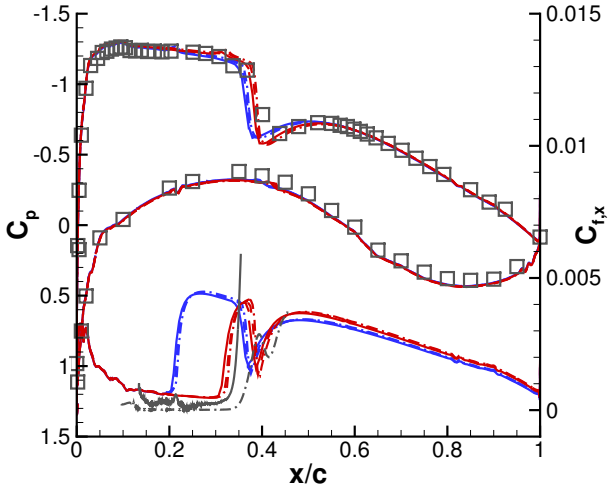


(e) 1.2 degrees

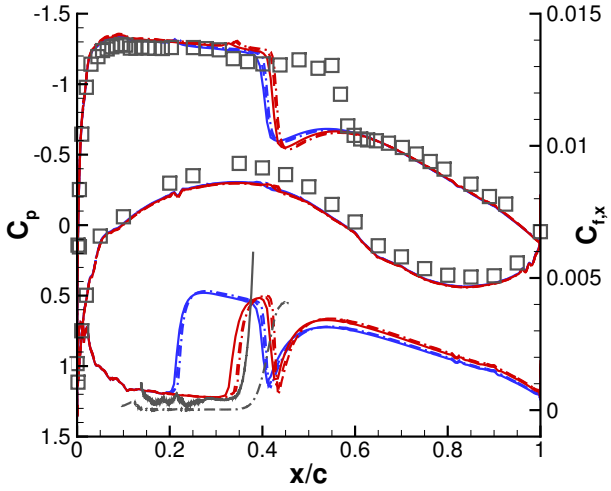


(f) 1.5 degrees

- At higher angles of attack the wind tunnel effects become significant.
- Good agreement is observed between the unscaled laminar skin friction coefficient and simulation.



(g) 1.8 degrees



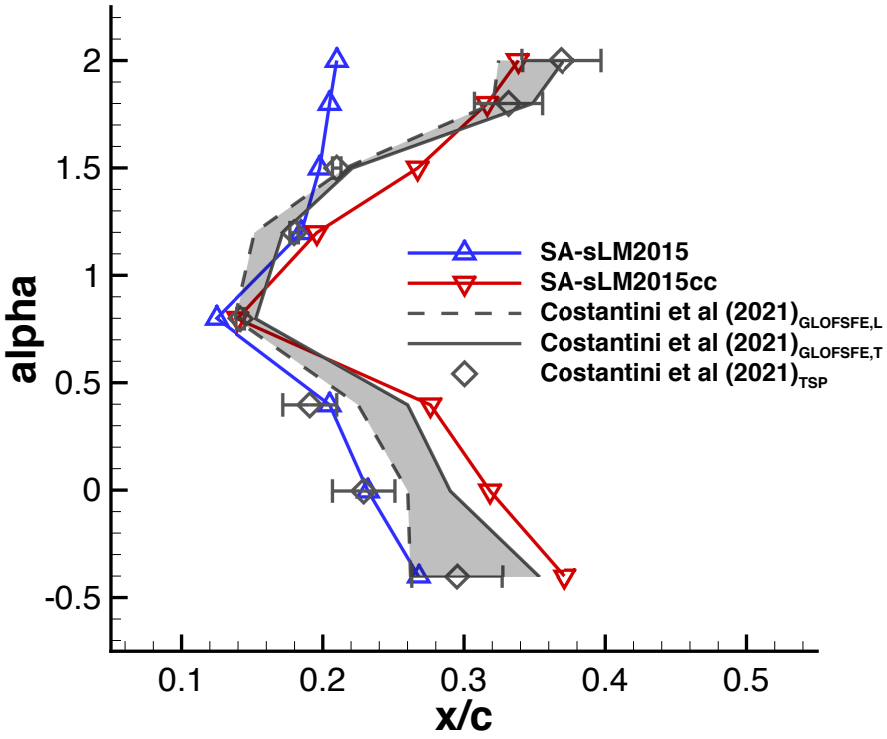
(h) 2.0 degrees

Institute for Aerospace Studies
UNIVERSITY OF TORONTO
Centre for Research in Sustainable Aviation

Transonic Validation: VA-2 Airfoil

Alpha Sweep: Upper Surface Transition Locations

M = 0.71 Tu = 0.25%
α = -0.4 - 2.0°
Re = 10.0x10^6



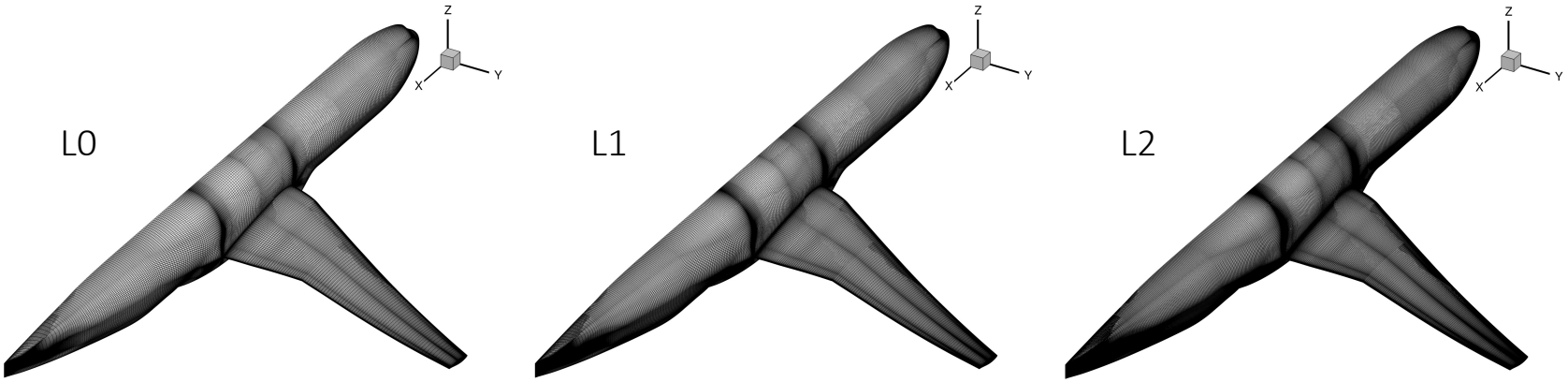
Upper surface predicted transition locations compared with experimental results obtained using temperature sensitive paint (TSP) and oil-film methods (GLOFSFE) (Costantini et al 2021).

- The transition model with the compressibility correction, SA-sLM2015cc, in general agrees best with the end of transition locations identified using the oil-film experiments.

Transonic Validation: NASA CRM-NLF

M = 0.86 Tu = 0.24%
α = 2° h_{rms} = 1x10^{-6}in
Re = 15.0x10^{6}

The smooth transition model with and without the compressibility corrections, SA-sLM2015cc and SA-sLM2015, respectively, is applied to the transonic NASA CRM-NLF transition test case (Lynde et al 2019)



grid level	# of nodes	average/maximum $\Delta s \times 10^{-6}$ (chord)	average/maximum $y+$
L0	8,893,456	1.00 / 2.24	0.36 / 1.50
L1	16,691,200	0.78 / 1.75	0.28 / 1.06
L2	32,787,200	0.60 / 1.35	0.22 / 0.78

- A full validation study including two-dimensional transonic transition test cases will be presented in an upcoming publication[2]

[2]Piotrowski, M.G.H., and Zingg, D.W., "Compressibility Corrections to Extend a Smooth Local Correlation-Based Transition Model to Transonic Flows" *Submitted*

Transonic Validation: NASA CRM-NLF

Grid Refinement Study: Upper Surface Skin Friction Coefficient Profiles

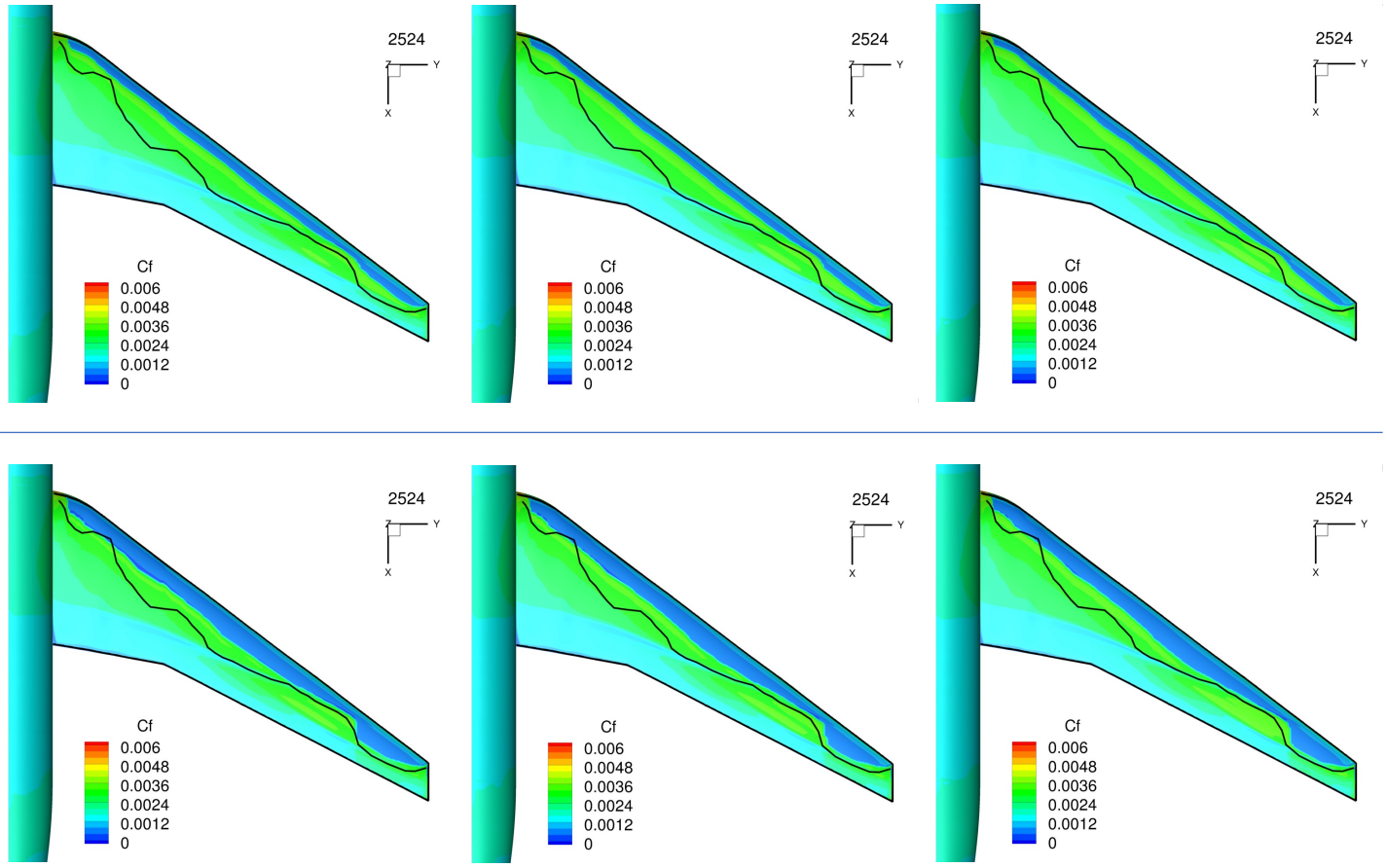
M = 0.86 Tu = 0.24%

α = 2° h_{rms} = $1x10^{-6}$in

Re = $15.0x10^{6}$

SA-sLM2015

SA-sLM2015cc



(a) L0 (b) L1 (c) L2

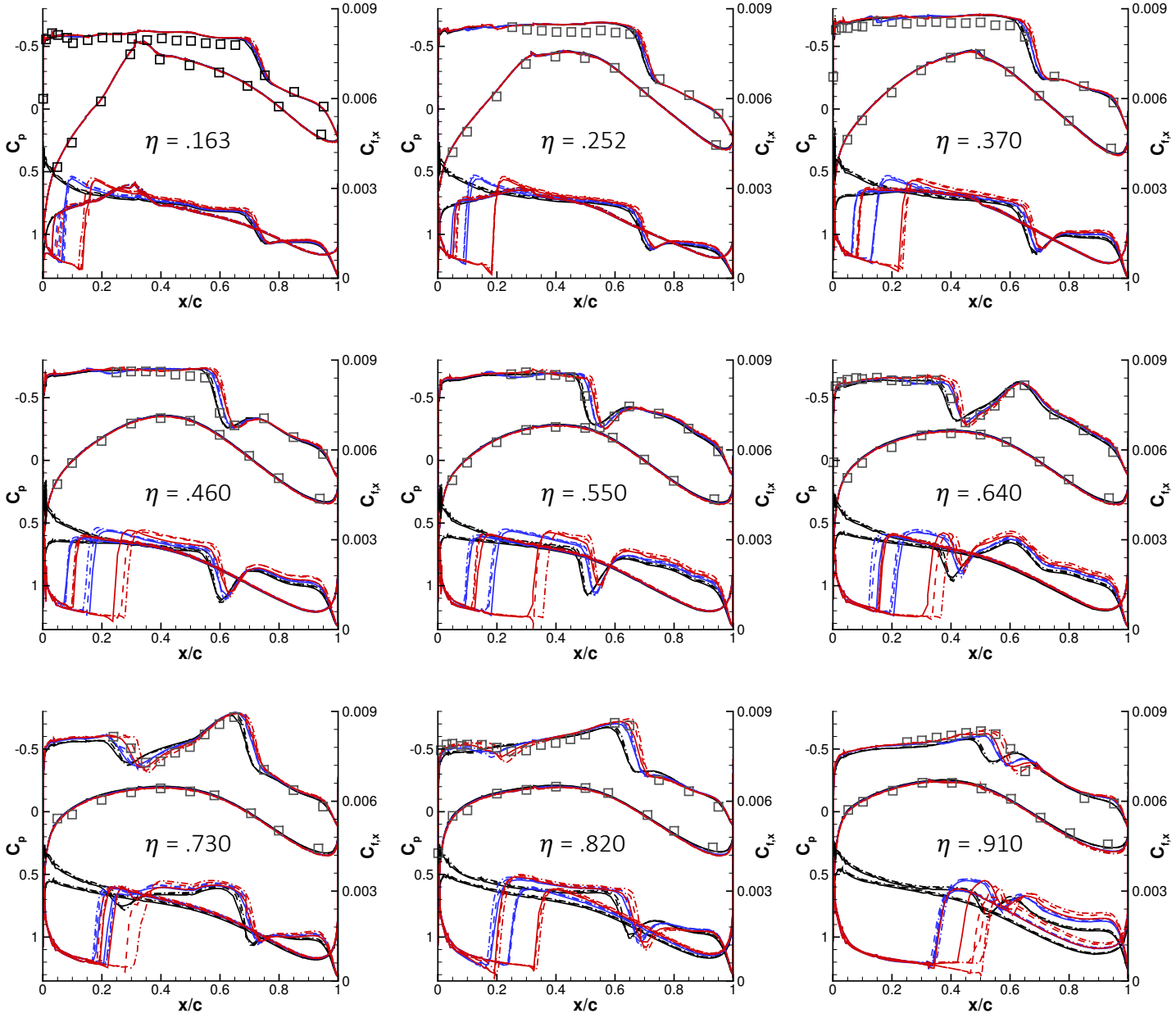
- Skin-friction profiles produced by the SA-sLM2015 and SA-sLM2015cc transition models overlaid with the experimental results, Lynde et al (2019).
- Compressibility corrections successfully delay transition to agree well with experiment.

Transonic Validation: NASA CRM-NLF

Grid Refinement Study: Cross-Sectional Profiles

M = 0.86
α = 2°
Re = 15.0x10^6

Tu = 0.24%
h_{rms} = 1x10^{-6}in



- Increased laminar extent of the boundary layer delays shock to better agree with experiment.
- Particularly evident at outboard stations η = 0.64 – 0.91.

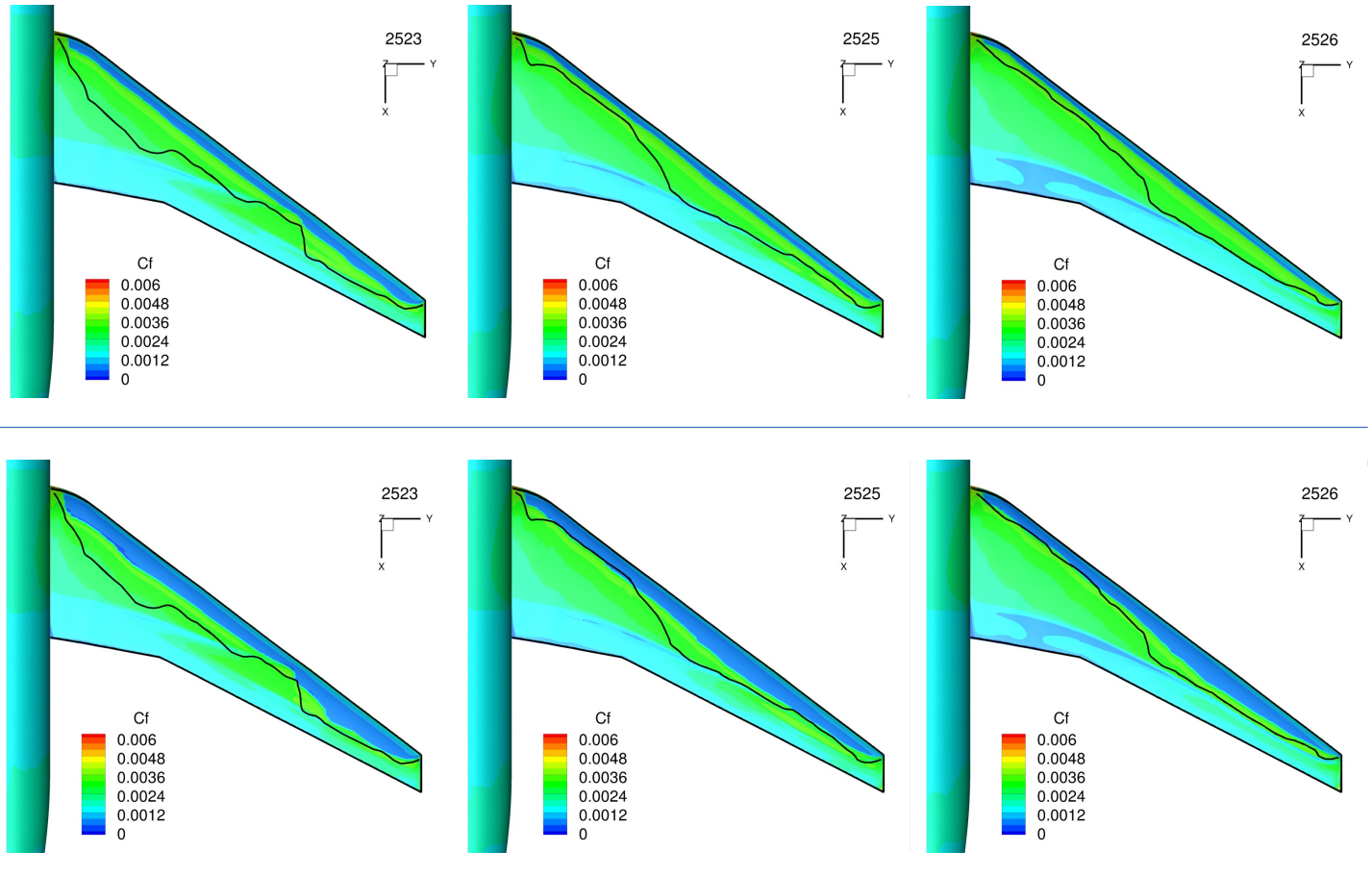
Transonic Validation: NASA CRM-NLF

Alpha Sweep: Upper Surface Skin Friction Coefficient Profiles

M = 0.86 Tu = 0.24%
α = 1.5 - 3.0° h_{rms} = 1x10^{-6}in
Re = 15.0x10^{6}

SA-sLM2015

SA-sLM2015cc



(a) 1.5° (b) 2.5° (c) 3.0°

- Skin friction profiles produced by the SA-sLM2015 and SA-sLM2015cc transition models on the L1 grid level, overlaid with the experimental results (Lynde et al 2019).
- Compressibility corrections successfully delay transition to agree well with experiment.

Optimization: Gradient Calculation

The discrete-adjoint Lagrangian function for the PDE-constrained optimization problem containing the flow and mesh adjoint variables is given by,

$$L(Q, C, X, \psi_\mathrm{f}, \psi_\mathrm{m}) = J(Q, C, X) - \psi_\mathrm{f}^T(R(Q, C, X)) - \psi_\mathrm{m}^T M(C, X).$$

- Setting the first derivatives of the Lagrangian with respect to Q, C, X, φ_f, and φ_m to zero we recover the first-order optimality conditions:

Mesh deformation: $$\frac{\partial L}{\partial \psi_\mathrm{m}} = 0 = M(C, X),$$

Discrete flow problem: $$\frac{\partial L}{\partial \psi_\mathrm{f}} = 0 = R(Q, C, X),$$

Flow adjoint problem: $$\frac{\partial L}{\partial Q} = 0 = \frac{\partial J}{\partial Q} - \psi_\mathrm{f}^T \frac{\partial R}{\partial Q},$$

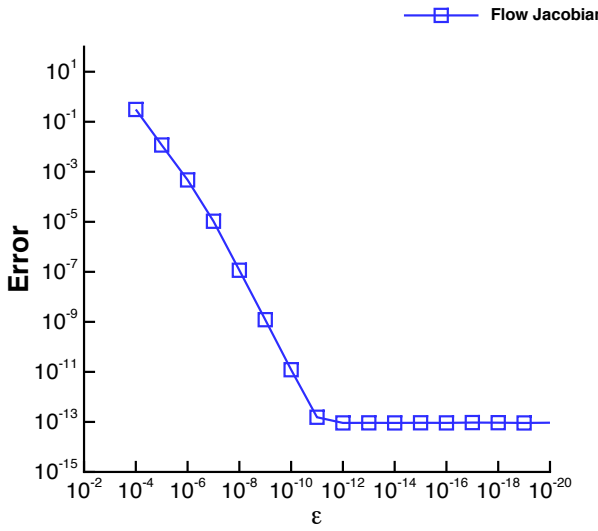
Mesh adjoint problem: $$\frac{\partial L}{\partial C} = 0 = \frac{\partial J}{\partial C} - \psi_\mathrm{f}^T \frac{\partial R}{\partial C} - \psi_\mathrm{m}^T \frac{\partial M}{\partial C},$$

The gradient: $$\frac{\partial L}{\partial X} = 0 = \frac{\partial J}{\partial X} - \psi_\mathrm{f}^T \frac{\partial R}{\partial X} - \psi_\mathrm{m}^T \frac{\partial M}{\partial X}.$$

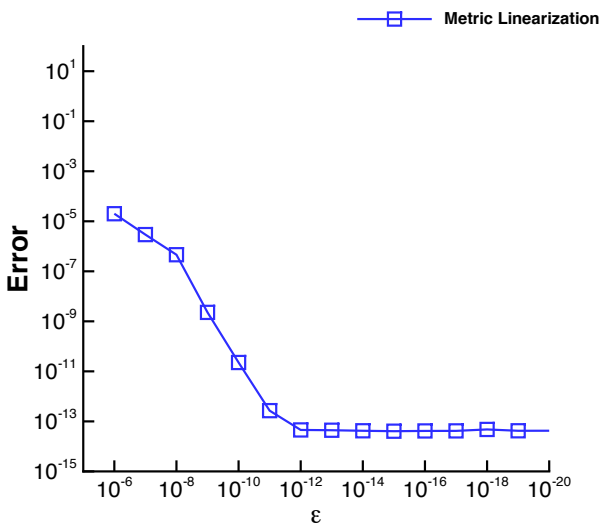
- Partial derivatives are formed analytically using hand linearization with some entries determined using the complex-step method.

Optimization: Flow Jacobian and Metric Linearization

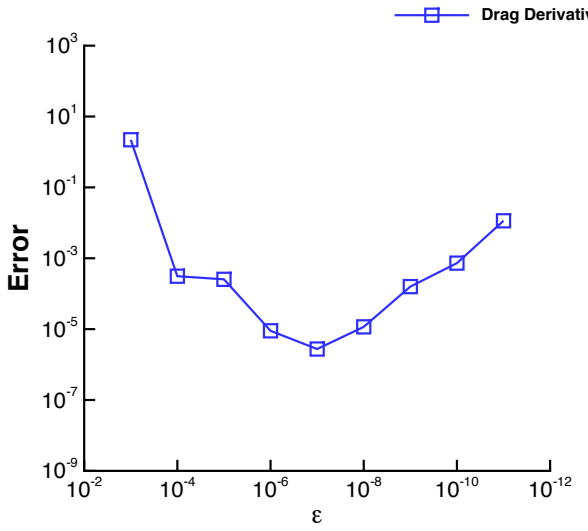
The flow Jacobian and metric linearization are each verified through comparing with the complex-step method, while the analytical gradient is verified using a finite-difference approximation.



(a) Flow Jacobian



(b) Metric Linearization



(c) Gradient

- Machine-zero agreement is demonstrated for both the analytical flow Jacobian and metric linearization with approximations formed using the complex-step method.
- Good agreement is demonstrated between the analytical gradient and a finite-difference approximation.

Optimization: Problem Definitions

Lift-constrained drag-minimization studies of an RAE2822 airfoil.

- Design flight conditions representative of a Cessna 172R, De Havilland Dash8-Q400, and Boeing 737-800 aircraft.
- Shape control provided using section shape design variables, as well as angle of attack, with the cross-sectional area constrained to not decrease.
- Static geometry control with 6 free-form deformation volume design variables on each of the upper and lower surfaces.

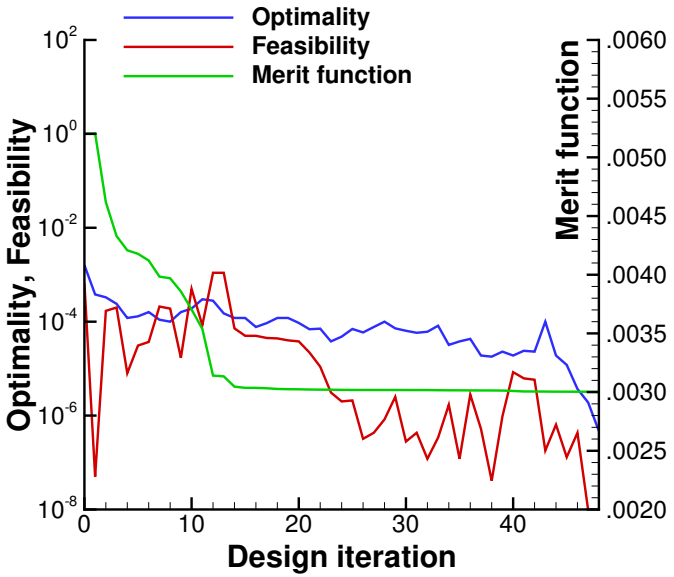
$$
\begin{aligned}
\min_{X} \quad & C_d(Q, X) \\
\text{s.t.} \quad & C_l = C_l^* \\
& A \geq A_{\text{init}} \\
& t/c \geq 0.15 t/c_{\text{init}}
\end{aligned}
$$

design condition	lift coefficient	Mach number	Reynolds number (MAC)
Cessna 172R	0.30	0.19	5.6×10^6
De Havilland Dash8-Q400	0.42	0.60	15.7×10^6
Boeing 737-800	0.50	0.71 (corr.)	20.3×10^6

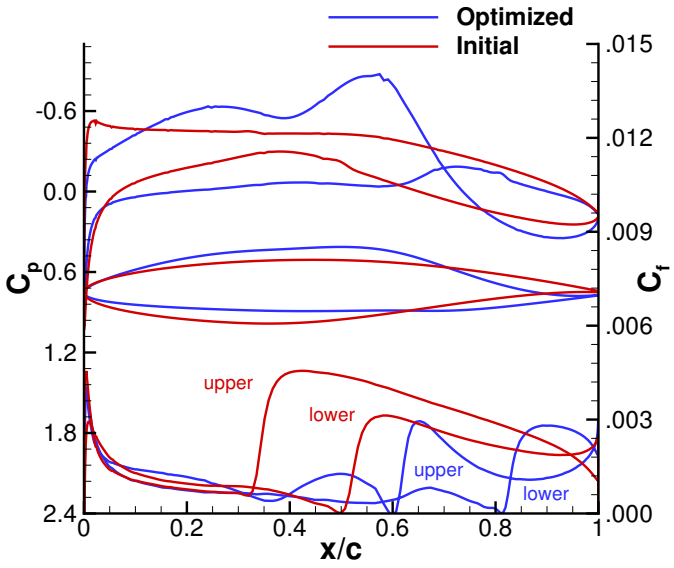
Optimization: Cessna 172R

Exploratory Design Problem

M = 0.19 Tu = 0.07%
Re = 5.6×10^6 C_l = 0.30



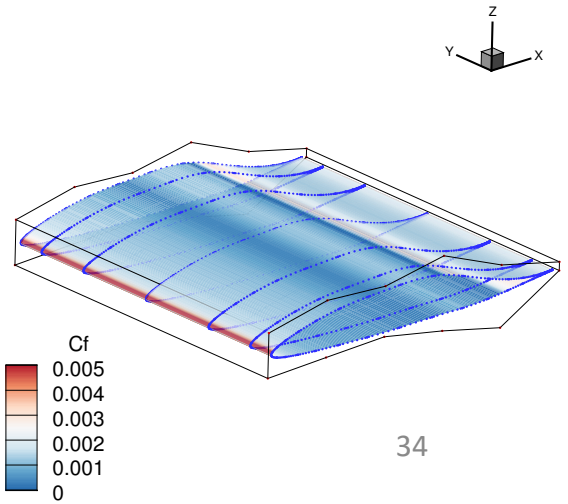
(a) Optimization history



(b) Cross-sectional profiles of the initial and optimized designs

$$\min_X \quad C_d(Q, X)$$
$$\text{s.t.} \quad C_l = C_l^*$$
$$A \geq A_{\text{init}}$$
$$t/c \geq 0.15 t/c_{\text{init}}$$

- ~43% reduction in drag.
- Transition front moved to 60% and 80% chord on the upper and lower surfaces, respectively.
- Undesirable performance at off-design conditions.

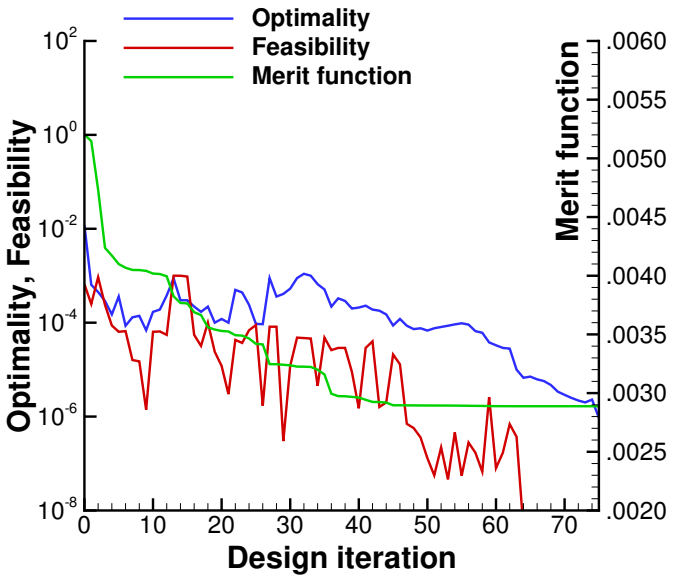


Institute for Aerospace Studies
UNIVERSITY OF TORONTO
Centre for Research in Sustainable Aviation

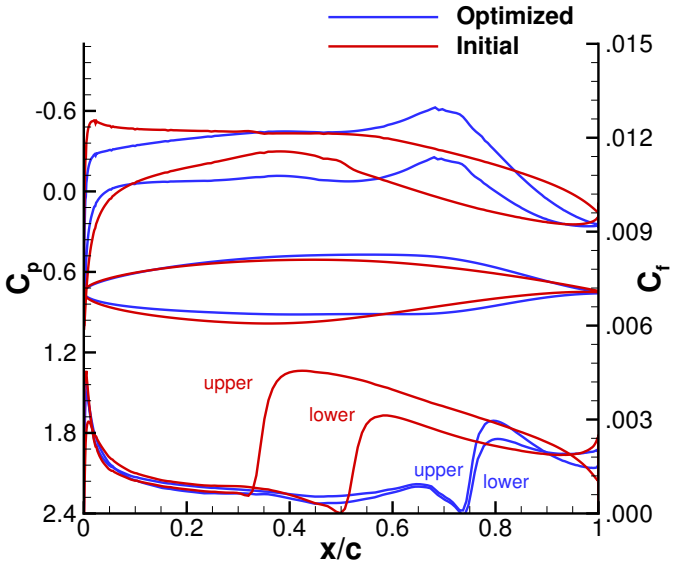
Optimization: Cessna 172R

More Practical Design Problem

M = 0.19 Tu = 0.07%
Re = 5.6×10^6 C_l = 0.30



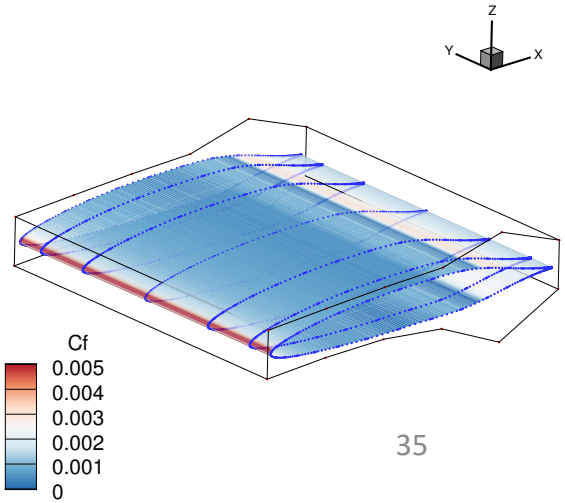
(a) Optimization history



(b) Cross-sectional profiles of the initial and optimized designs

$$\min_X \quad C_d(Q, X)$$
$$\text{s.t.} \quad C_l = C_l^*$$
$$C_m = C_{m,\text{init}}$$
$$A \geq A_{\text{init}}$$
$$t/c \geq 0.85 t/c_{\text{init}}$$

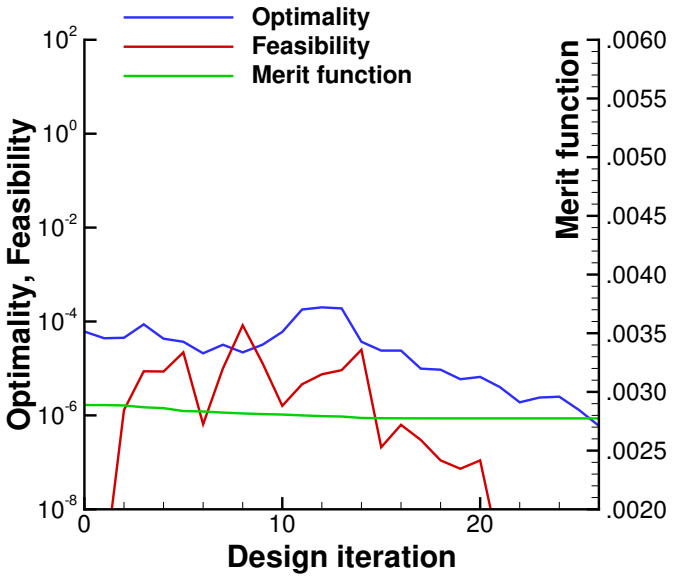
- ~45% reduction in drag
- Transition front moved to 75% chord on both the upper and lower surfaces.
- More practical design problem produces a better performing design.



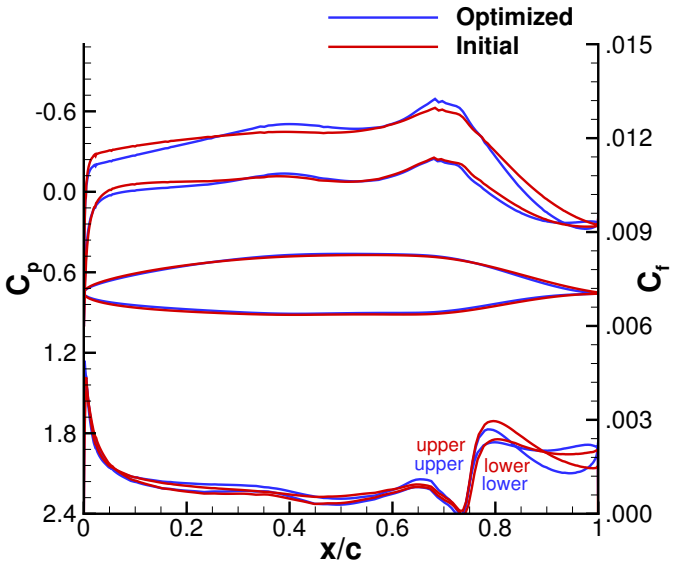
Optimization: Cessna 172R

More Practical Design Restarted with Exploratory Design Problem

M = 0.19 Tu = 0.07%
Re = 5.6×10^6 C_l = 0.30



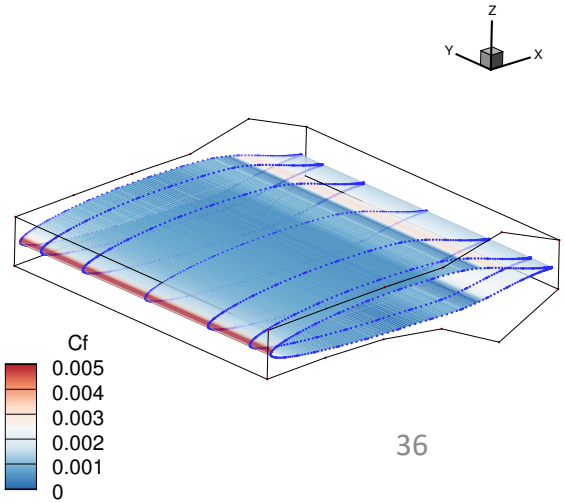
(a) Optimization history



(b) Cross-sectional profiles of the initial and optimized designs

$$\min_X \quad C_d(Q, X)$$
$$\text{s.t.} \quad C_l = C_l^*$$
$$A \geq A_{\text{init}}$$
$$t/c \geq 0.15 t/c_{\text{init}}$$

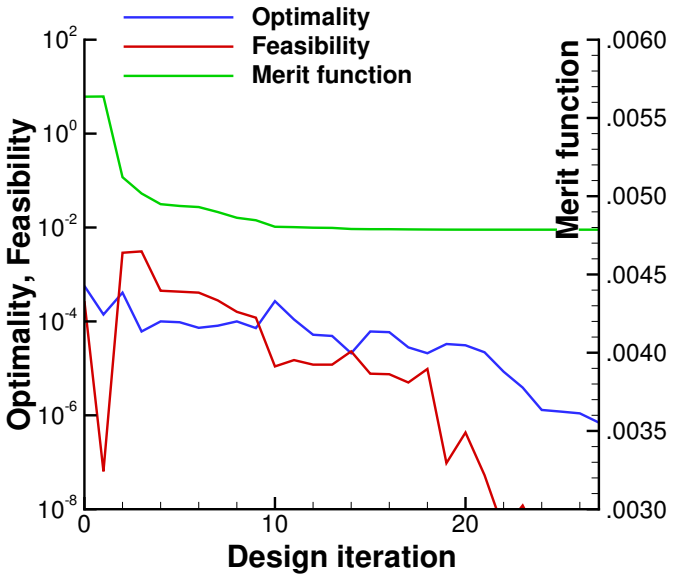
- Drag is reduced by an additional count.
- The results suggest that the Cessna 172R design condition is multi-modal.
- More practical design is similar to the design produced by Rashad and Zingg (2016).



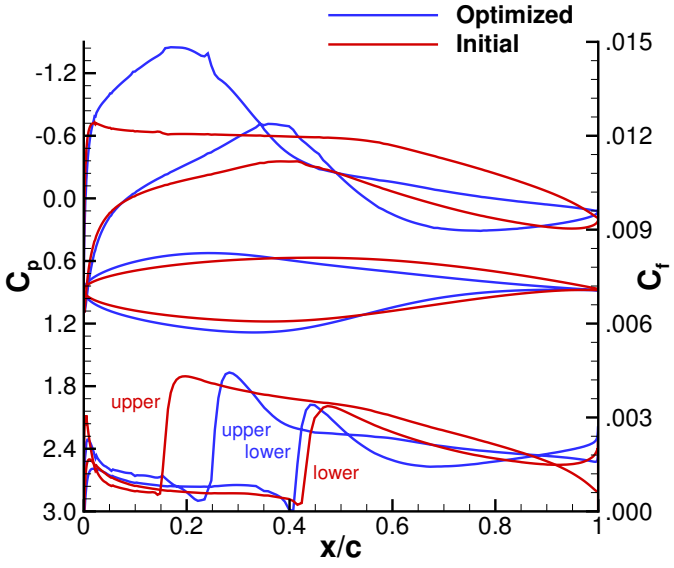
Optimization: De Havilland Dash8-Q400

Exploratory Design Problem: L0 – Baseline grid

M = 0.60 Tu = 0.07%
Re = 15.7x10^6 C_l = 0.42



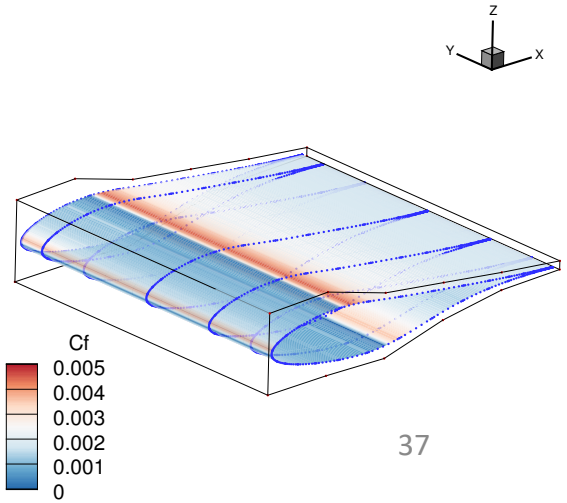
(a) Optimization history



(b) Cross-sectional profiles of the initial and optimized designs

$$\min_X \quad C_d(Q, X)$$
$$\text{s.t.} \quad C_l = C_l^*$$
$$A \geq A_{\text{init}}$$
$$t/c \geq 0.15 t/c_{\text{init}}$$

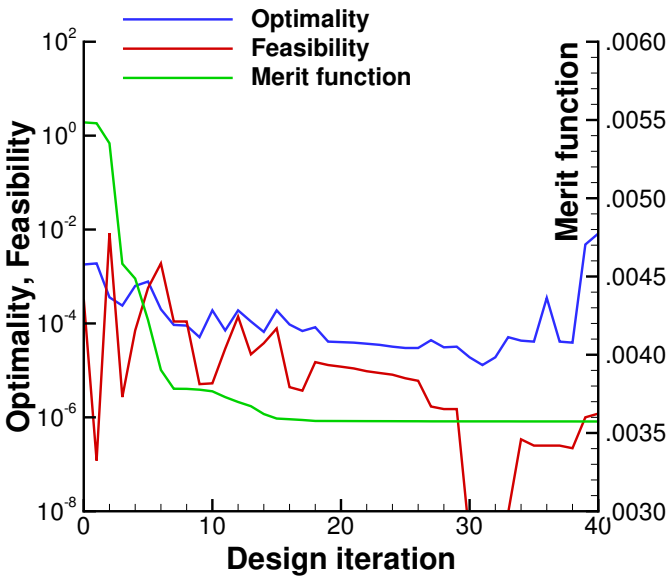
- Higher Reynolds number decreases transition region length.
- Optimizer develops adverse pressure gradients to reduce the turbulent skin friction.
- Finer chordwise resolution is required in order to sufficiently resolve the gradients in the transition region.



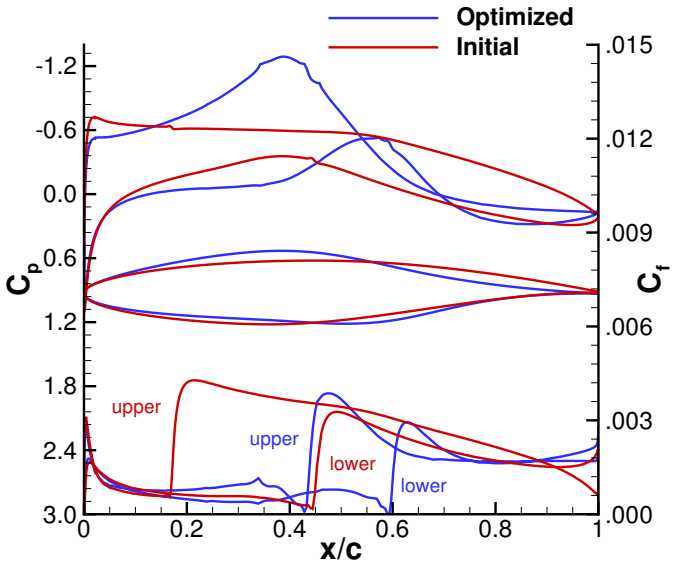
Optimization: De Havilland Dash8-Q400

Exploratory Design Problem : L1 – Double chordwise resolution

M = 0.60 Tu = 0.07%
Re = 15.7x10^6 C_l = 0.42



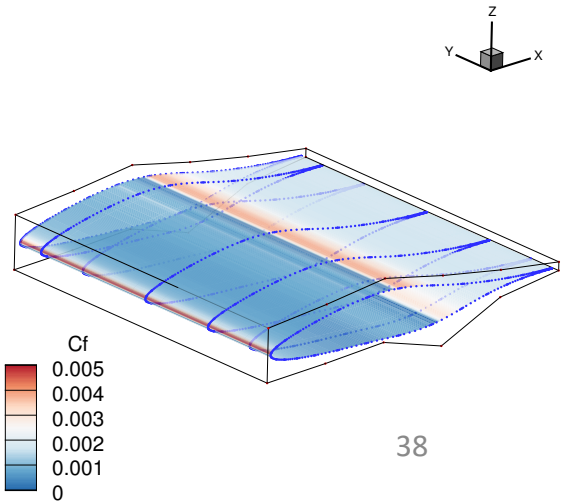
(a) Optimization history



(b) Cross-sectional profiles of the initial and optimized designs

$$\min_X \quad C_d(Q, X)$$
$$\text{s.t.} \quad C_l = C_l^*$$
$$A \geq A_{\text{init}}$$
$$t/c \geq 0.15 t/c_{\text{init}}$$

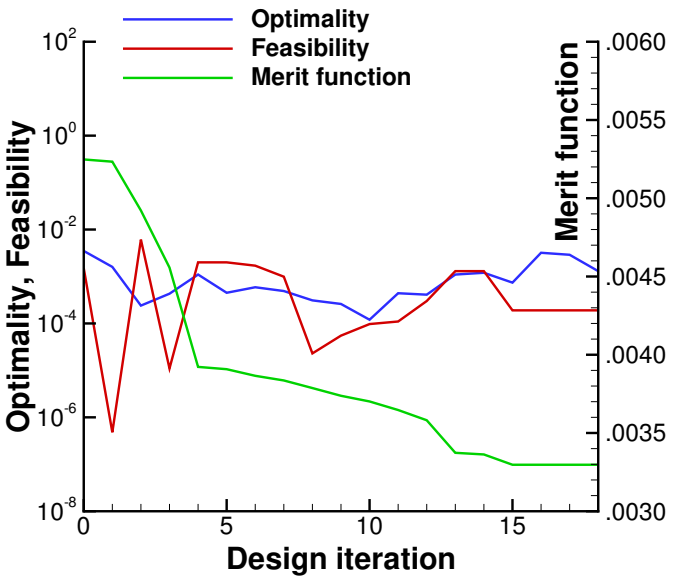
- The gradients in the transition region are better resolved as the chordwise grid resolution is increased.
- Transition locations are pushed downstream to ~40% and ~60% chord for the upper and lower surfaces, respectively.



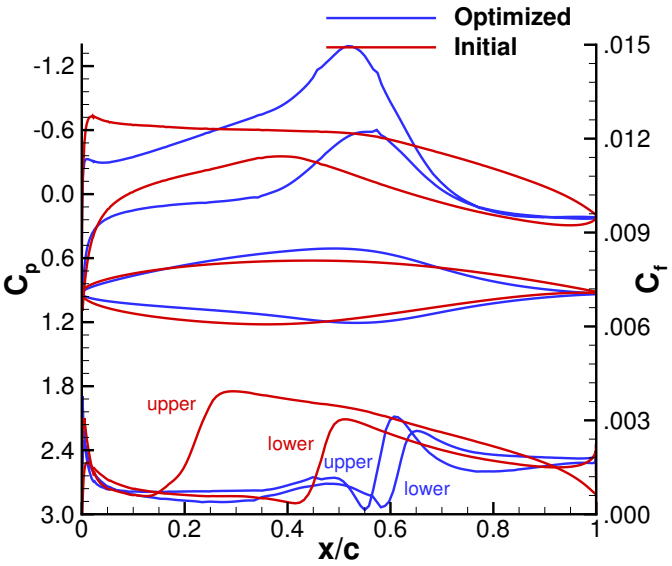
Optimization: De Havilland Dash8-Q400

Exploratory Design Problem : L0 – Baseline grid

M = 0.60 Tu = 0.07%
Re = 15.7x10^6 C_l = 0.42



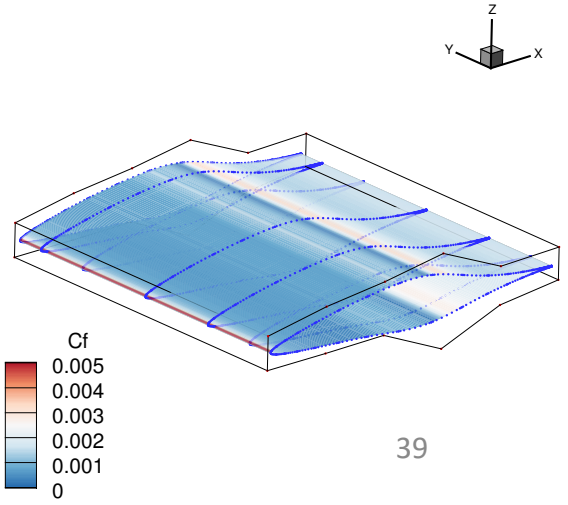
(a) Optimization history



(b) Cross-sectional profiles of the initial and optimized designs

$$\min_X \quad C_d(Q, X)$$
$$\text{s.t.} \quad C_l = C_l^*$$
$$A \geq A_{\text{init}}$$
$$t/c \geq 0.15 t/c_{\text{init}}$$

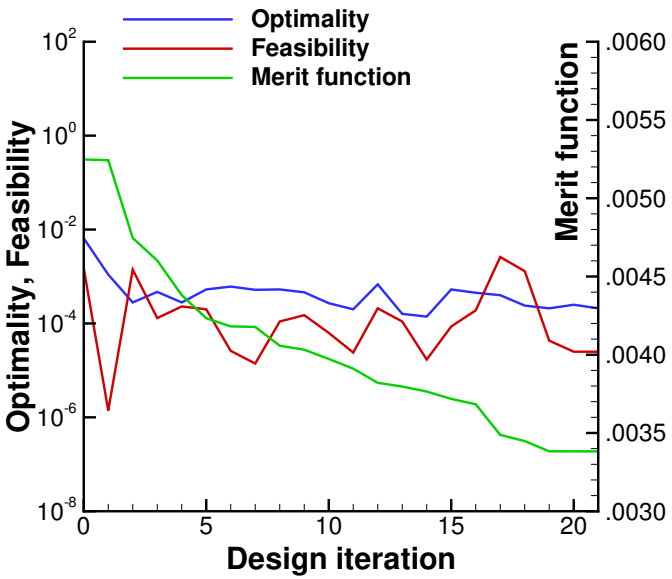
- Alternatively, increasing the transition region length reduces the grid requirements for the optimization.
- Increased resolution in the transition region improves the performance of the optimization algorithm.



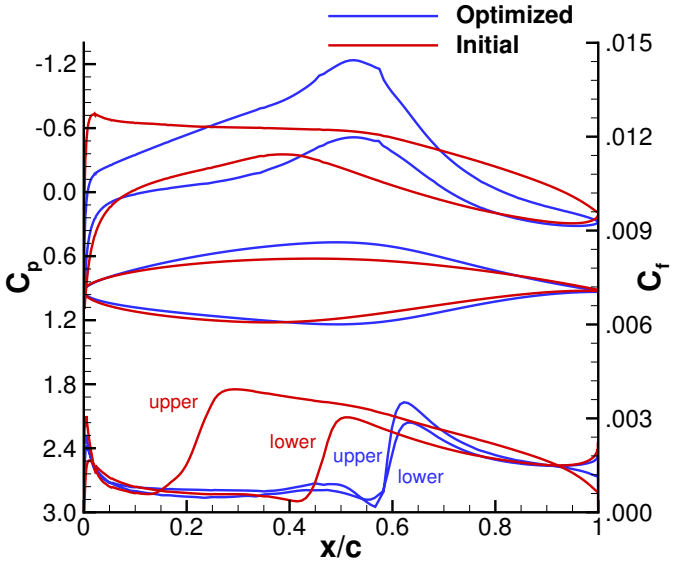
Optimization: De Havilland Dash8-Q400

More Practical Design Problem: L0 – Baseline grid

M = 0.60 Tu = 0.07%
Re = 15.7x10^6 C_l = 0.42



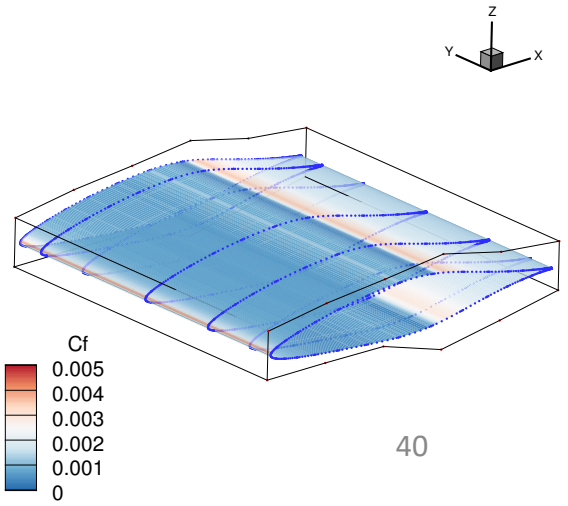
(a) Optimization history



(b) Cross-sectional profiles of the initial and optimized designs

$$\min_X \quad C_d(Q, X)$$
$$\text{s.t.} \quad C_l = C_l^*$$
$$C_m = C_{m,\text{init}}$$
$$A \geq A_{\text{init}}$$
$$t/c \geq 0.85 t/c_{\text{init}}$$

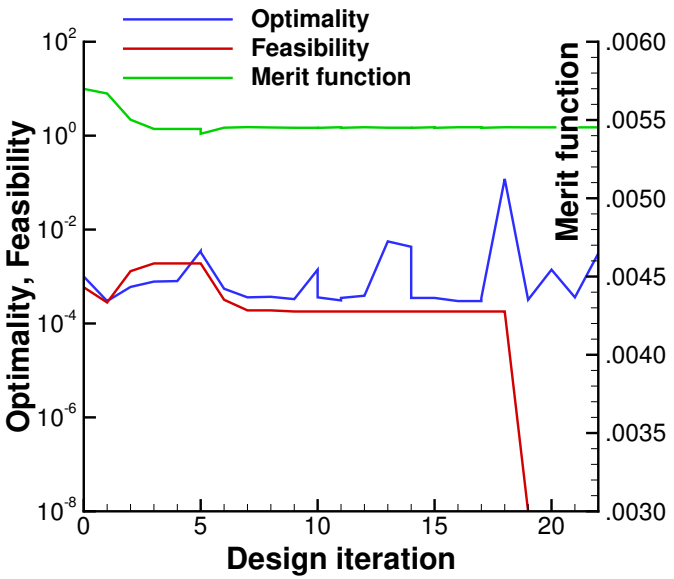
- The more practical design problem produces a more conservative design with a small penalty to performance.
- ~36% reduction in drag.



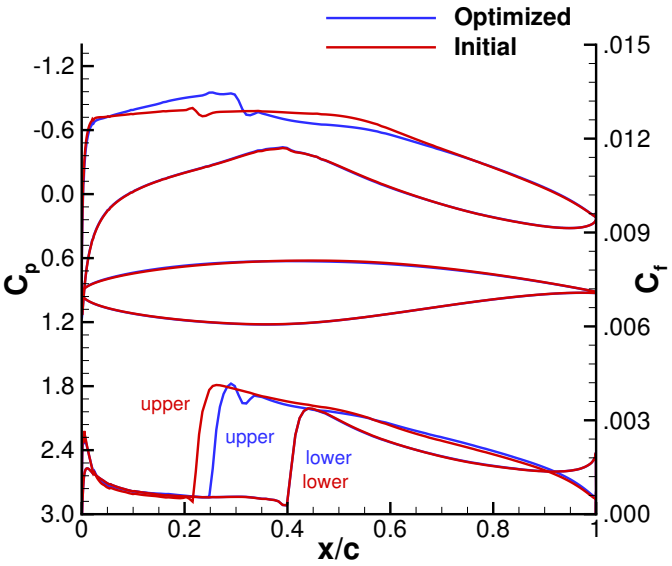
Optimization: Boeing 737-800

More Practical Design Problem

M = 0.71 (corr.) Tu = 0.07%
Re = 20.3×10^6 $C_l = 0.50$



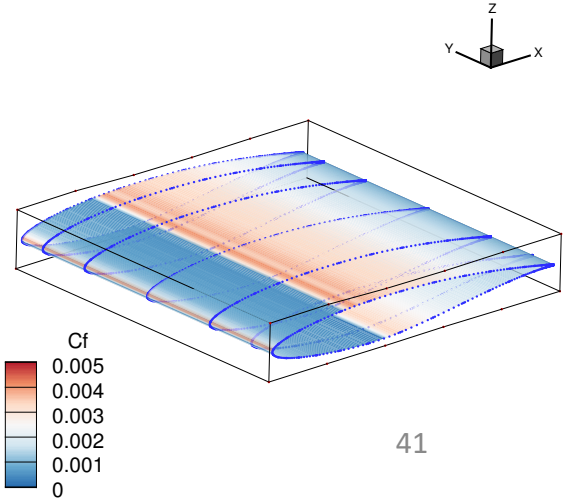
(a) Optimization history



(b) Cross-sectional profiles of the initial and optimized designs

$$\begin{aligned} \min_X \quad & C_d(Q, X) \\ \text{s.t.} \quad & C_l = C_l^* \\ & C_m = C_{m,\text{init}} \\ & A \geq A_{\text{init}} \\ & t/c \geq 0.85 t/c_{\text{init}} \end{aligned}$$

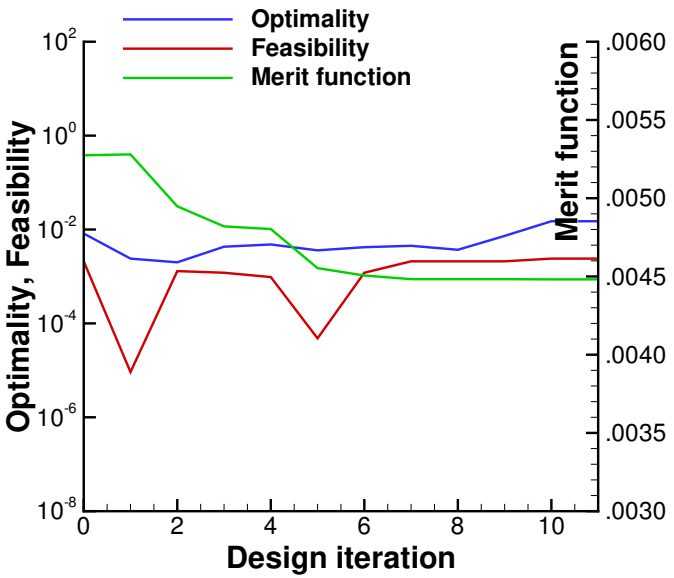
- At the higher Reynolds number, the transition length is further reduced.
- Optimizer is demonstrating difficulty in trading viscous drag and wave drag.
- Current optimizations do not include the effect of crossflow instabilities.



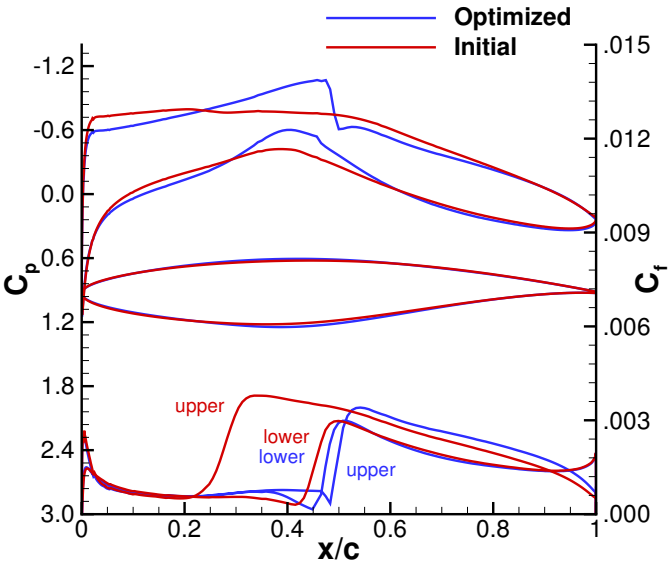
Optimization: Boeing 737-800

More Practical Design Problem

M = 0.71 (corr.) Tu = 0.07%
Re = 20.3×10^6 $C_l = 0.50$



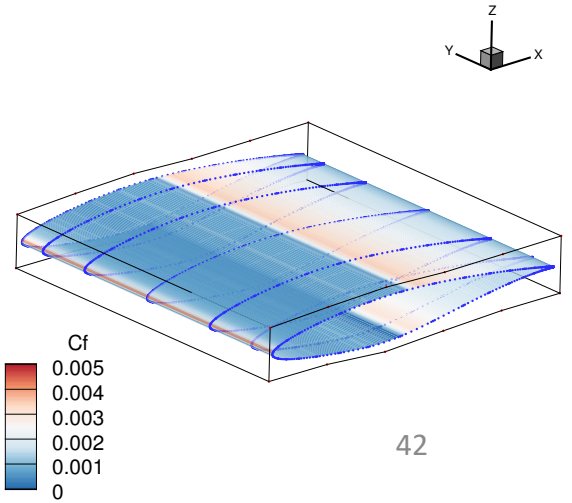
(a) Optimization history



(b) Cross-sectional profiles of the initial and optimized designs

$$\min_X \quad C_d(Q, X)$$
$$\text{s.t.} \quad C_l = C_l^*$$
$$C_m = C_{m,\text{init}}$$
$$A \geq A_{\text{init}}$$
$$t/c \geq 0.85 t/c_{\text{init}}$$

- Increasing the transition region length provides a smoother design space.
- Optimizer trades a decrease in viscous drag with an increase in wave drag.
- Ongoing work is focused on infinite swept wing optimizations in order to include the effects of crossflow instabilities.



Summary

Objectives:

1. Extension of a three-dimensional RANS solver with a local laminar-turbulent transition prediction model.
   - SA-LM2015 transition model developed and validated.
2. Develop a framework for achieving deep, efficient convergence.
   - Source-term time stepping.
   - Smooth-variant developed, SA-sLM2015, which improves numerical behavior.
3. Validate model for transonic flow regimes typical of commercial transport aircraft.
   - Compressibility corrections developed for empirical correlations, SA-sLM2015cc.
   - Validated for two- and three-dimensional transonic transition test cases.
4. Integrate in a discrete-adjoint gradient-based optimization algorithm and apply to drag-minimization studies.
   - Verified gradient and partial derivatives.
   - Preliminary airfoil optimizations demonstrate capabilities of resulting algorithm.

Future Work:

1. Infinite swept wing optimizations at the Boeing 737-800 design conditions to investigate the interaction between Tollmien-Schlichting and crossflow instabilities.
2. Transonic NLF wing optimizations to explore the transonic NLF wing design space including the trade-offs between viscous drag and wave drag.

Acknowledgements

- This work was partially funded by the NASA Transformational Tools and Technologies (TTT) and Advanced Air Transport Technology (AATT) projects, the Natural Sciences and Engineering Research Council (NSERC), and the University of Toronto.
- Computations were performed on the Niagara supercomputer at the SciNet HPC Consortium, a part of Compute Canada.
- The authors gratefully acknowledge the input and support provided by Dr. Thomas Reist, Dr. Cetin Kiris, and the LAVA team.